Journal of Controlled Release 334 (2021) 138–152

Contents lists available at ScienceDirect

Journal of Controlled Release

journal homepage: www.elsevier.com/locate/jconrel

Non-viral gene delivery of the oncotoxic protein NS1 for treatment of hepatocellular carcinoma

Dominik Witzigmann [a,b,1], Philip Grossen [a,1], Cristina Quintavalle [c], Manuela Lanzafame [c], Susanne H. Schenk [a], Xue-Ting Tran [a], Bernhard Englinger [d], Patrick Hauswirth [a], David Grünig [e], Sushilla van Schoonhoven [d], Stephan Krähenbühl [e], Luigi M. Terracciano [c], Walter Berger [d], Salvatore Piscuoglio [c,f], Luca Quagliata [c], Jean Rommelaere [g], Jürg P.F. Nüesch [g], Jörg Huwyler [a,*]

[a] Division of Pharmaceutical Technology, Department of Pharmaceutical Sciences, University of Basel, 4056 Basel, Switzerland
[b] Department of Biochemistry and Molecular Biology, University of British Columbia, Health Sciences Mall, V6T 1Z3 Vancouver, British Columbia, Canada
[c] Institute of Pathology, Molecular Pathology Division, University Hospital of Basel, 4003 Basel, Switzerland
[d] Applied and Experimental Oncology, Institute of Cancer Research and Comprehensive Cancer Center, Medical University of Vienna, 1090 Vienna, Austria
[e] Division of Clinical Pharmacology and Toxicology, University Hospital of Basel, 4031 Basel, Switzerland
[f] Visceral Surgery laboratory, Clarunis, Department of Biomedicine, 4031 Basel, Switzerland
[g] Infection, Inflammation and Cancer Program, Division of Tumor Virology, German Cancer Research Center (DKFZ), 69120 Heidelberg, Germany

ARTICLE INFO

Keywords:
Hepatocellular carcinoma
Gene therapy
Parvovirus
Nanoparticles
Oncotoxic protein

ABSTRACT

Hepatocellular carcinoma (HCC) is related to increasing incidence rates and poor clinical outcomes due to lack of efficient treatment options and emerging resistance mechanisms. The aim of the present study is to exploit a non-viral gene therapy enabling the expression of the parvovirus-derived oncotoxic protein NS1 in HCC. This anti-cancer protein interacts with different cellular kinases mediating a multimodal host-cell death. Lipoplexes (LPX) designed to deliver a DNA expression plasmid encoding NS1 are characterized using a comprehensive set of *in vitro* assays. The mechanisms of cell death induction are assessed and phosphoinositide-dependent kinase 1 (PDK1) is identified as a potential predictive biomarker for a NS1-LPX-based gene therapy. In an HCC xenograft mouse model, NS1-LPX therapeutic approach results in a significant reduction in tumor growth and extended survival. Data provide convincing evidence for future studies using a targeted NS1 gene therapy for PDK1 overexpressing HCC.

1. Introduction

Despite recent advances in cancer diagnosis and treatment options, therapeutic interventions for several malignancies are still insufficient. For example, mortality rates of HCC are increasing annually by 2.7% (women) and 1.6% (men) accounting for 3% or 6% of cancer related deaths in the United states [1]. Current treatment options in accordance to the Barcelona Clinic Liver Cancer (BCLC) staging system, *i.e.* surgical resection, systemically and locally applied chemotherapy or radio-embolization, show only limited success and thus new therapeutic strategies are urgently needed [2,3].

Recently, anticancer genes and their proteins that selectively induce cell death in malignant cells have gained much attention and hallmark a new era of cancer treatment [4–6]. For example, the 14 kDa protein apoptin from the Chicken anemia virus was tested on various human tumor cell lines and efficiently induced apoptosis [7,8]. In contrast, no or only minor effects were observed in healthy cells such as primary hepatocytes [9]. Another interesting candidate is derived from the rat parvovirus (H-1PV). H-1PV is a Protoparvovirus of rodent (rat or hamster) origin, isolated as an opportunistic infectant in a human cancer cell line [10] and was shown to infect, propagate in and kills both, transformed rat and human cancer cell lines [11,12]. This virus showed promising results in the treatment of various tumors in a preclinical setting [13]. The major effector protein of H-1PV is the large non-

* Corresponding author.
E-mail address: joerg.huwyler@unibas.ch (J. Huwyler).
[1] These authors contributed equally.

https://doi.org/10.1016/j.jconrel.2021.04.023
Received 28 July 2020; Received in revised form 10 April 2021; Accepted 20 April 2021
Available online 22 April 2021

structural protein 1 (NS1) consisting of 672 amino acids [14]. Interestingly, NS1 is not only essential for viral replication, but the expression of NS1 without other viral components is sufficient to kill cancer cells [15–17]. NS1 induces multimodal cell death *via* apoptosis, necrosis, and lysosomal-like cell death exclusively in neoplastically transformed (tumor) cells [18–20]. Consequently, a H-1PV-based therapy for the treatment of patients suffering from glioblastoma multiforme is at present tested in a clinical Phase-I/IIa trial (ParvOryx01, NCT01301430) [21,22]. However, despite promising results using oncotoxic viruses, virus-based therapies have several drawbacks and raise safety concerns with respect to virus replication, insertional mutagenesis, genetic stability (*e.g.* loss of specificity), and immunogenicity [23,24]. Thus, delivery of virus-derived anticancer genes using non-viral vectors could expand the therapeutic potential and safety of such promising concepts.

Nanomedicines have evolved in recent years and more than 10 nanodrug formulations have received market approval, mostly for the treatment of malignant diseases [25]. Lipid-based nanoparticles are among the most advanced systems for systemic and local gene therapy and several formulations aiming to deliver nucleic acids for RNA interference, cancer vaccination, or enzyme replacement therapies are currently in clinical trials [26–28].

The goal of the present study was therefore to combine the therapeutic potential of parvovirus-derived NS1 and the high plasmid DNA (pDNA) delivery capacity of LPXs after local administration for the treatment of HCC. For the first time, pDNA-loaded LPXs encoding the sequence of the oncotoxic protein NS1 (NS1-LPXs) were used for the treatment of HCC. In a first step, a set of nine human liver cancer-derived cell lines and primary human hepatocytes (PHH) were used to analyze: (1) the NS1-LPX cell interaction, (2) the expression and subcellular distribution of NS1, and (3) the selective therapeutic effect of NS1-LPXs in malignant cells. Noteworthy, therapeutic effects showed striking differences between the various cell lines tested and we categorized these according to their response rate. Second, the mechanisms of cell death induction in cells of each category (*i.e.* weakly, medium, and strongly responsive cells) were analyzed *in vitro* using a comprehensive set of assays. Third, a biomarker for patient stratification prior to therapy with NS1-LPXs was identified. Recently, it was shown by our group that growth-factor independent activation of PDK1 is essential for the intracellular activation of NS1 after viral delivery and consequently this master kinase was proposed as predictive biomarker for successful H-1PV therapy in glioma patients [29]. Indeed, expression of constitutively active PDK1 rendered weakly responsive liver cancer cells susceptible to NS1-LPX-based therapy. Consequently, a microarray analysis was performed to assess PDK1 mRNA and protein expression levels in HCC patients (tumoral and non-tumoral tissue). In a last step, NS1-LPXs were used to treat HCC in mice using a human xenograft model. In this proof-of-concept study, a significant reduction in tumor growth and extended survival were observed when mice were treated with NS1-LPXs as compared to mice treated with LPXs carrying a non-coding pDNA vector. Observed effects strongly correlated with expression of NS1.

2. Results and discussion

2.1. NS1-LPXs induce significant expression of NS1 in human liver cancer cells

The H-1PV-derived anticancer gene NS1 was cloned into the plasmid vectors pcDNA3.1 and pTagGFP-N to express NS1 or a NS1-GFP fusion

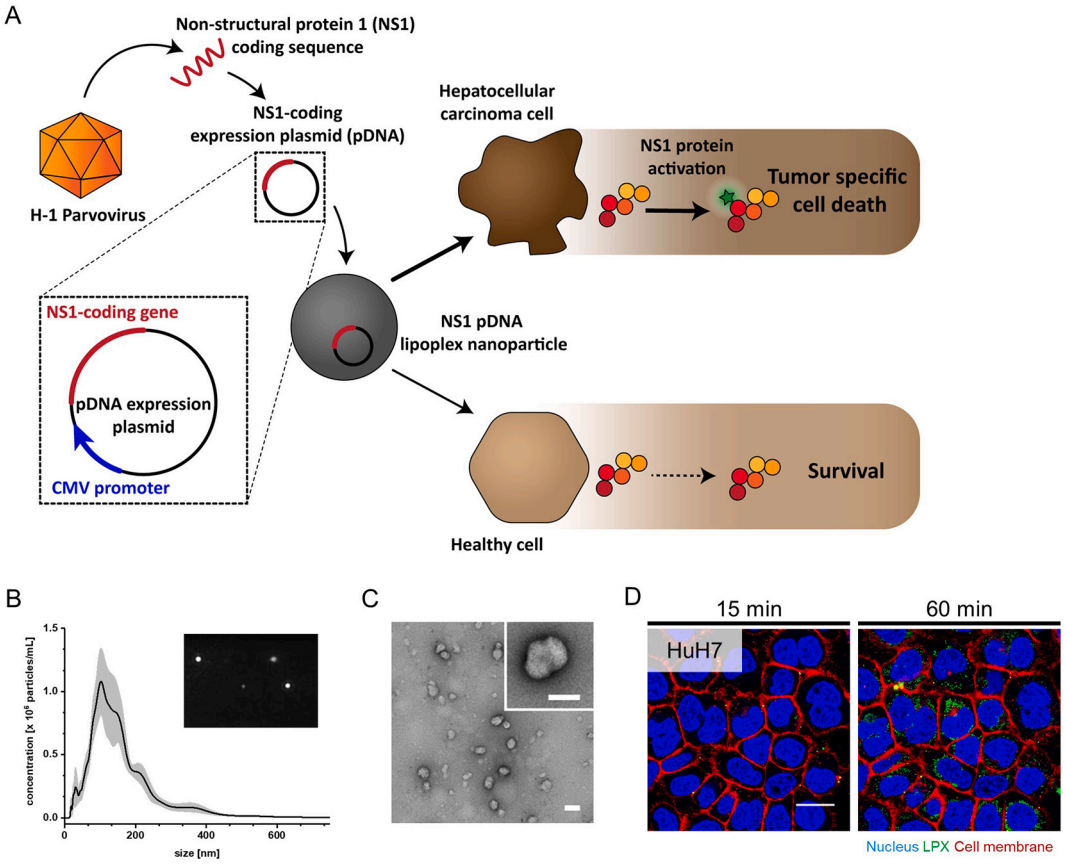

Fig. 1. NS1-LPXs are rapidly internalized *in vitro*. **A**, H-1 parvovirus-derived NS1 is cloned into an expression plasmid and delivered to liver cancer cells using lipoplexes (LPX). Selective activation of NS1 in tumor cells leads to cell death. **B**, Size distribution of NS1-LPXs based on nanoparticle tracking analysis. Means ± S.D. $N = 3$. Insert: representative image of a video sequence recorded during analysis. **C**, NS1-LPX nanoparticles. Representative transmission electron micrograph (uranyl acetate negative staining). Scale bar, 100 nm. **D**, Internalization of fluorescent LPXs by HuH7 cells analyzed by confocal microscopy. Scale bar, 20 μm.

protein in eukaryotic cells (Fig. 1A). A non-coding vector, *i.e.* empty vector, or GFP-coding pDNA vector were used as controls. The plasmid vectors were rapidly mixed with cationic lipid nanoparticles to induce spontaneous pDNA-LPX formation. LPXs had an average hydrodynamic diameter of 101.0 ± 2.6 nm (Fig. 1B) and were characterized by a positive zeta potential (11.6 ± 1.0 mV in phosphate buffered saline using a LPX:pDNA vector *V/w* ratio of 2) that is typical for lipoplexes [30]. Electron micrographs of LPXs confirmed these results, demonstrating spherical particles with an average size of 81.8 ± 27.0 nm ($N = 100$) and a monodisperse size distribution (Fig. 1C) corresponding to a polydispersity index of 0.109. Size, shape, and zeta potential did not change significantly for LPXs containing pDNA coding for GFP, NS1, NS1-GFP, or the empty vector. Fluorescently labeled LPXs (*i.e.* LPXs encapsulating fluorescently labeled pDNA) were internalized by human liver cancer-derived cell lines in a time-dependent manner (Fig. 1D and Fig. S1). All nine liver cancer-derived cell lines (HuH7, Hep3B, HLE, PLCPRF5, HuH6, SNU449, HepG2, SkHep1, and HepT1) expressed NS1, reaching gene expression efficiencies of up to 85% NS1-positive cells (Fig. 2A and B). Highest and most consistent transfection was reached in HuH7 cells. For all *in vitro* experiments, 0.1 ng pDNA/cell was used. NS1 expression was further confirmed by Western blot where a typical double band at 83 kDa was detected in all transfected cell lines (Fig. 2C and Fig. S2) [29]. In PV-infected cells, NS1 has a distinct intracellular distribution pattern and preferentially accumulates within specific foci in the cell nucleus during early phases of NS1 expression [31,32]. The intracellular distribution of NS1 after LPX delivery was therefore analyzed in absence of other viral proteins. Indeed, NS1-GFP accumulated in cell nuclei already 4 h after LPX uptake (Fig. 2D). NS1-GFP was detected in distinct nuclear foci and distributed in the nucleoplasm. The staining pattern is indicative for an absence of NS1-GFP from nucleoli as previously described for H-1PV (Fig. 2D and Fig. S3) [32]. These findings were additionally confirmed using immunofluorescence staining of NS1 (Fig. S4). Importantly, N-terminal fusion with GFP did not alter the intracellular distribution.

2.2. NS1 selectively induces cell death in cancer cells

H-1PV NS1 induces cytotoxic effects specifically in cancer cells indicating its oncotropism [18,19]. Since biopsies for diagnosis of HCC are not recommended and testing of freshly isolated patient material may thus raise ethical concerns, therapeutic effects of NS1-LPXs were assessed on a panel of nine human liver cancer-derived cell lines (Table S1) [33]. Since cationic nanoparticles are generally characterized by strong interactions with negatively charged cell surfaces [27], cytotoxic effects of NS1-LPXs were always compared to empty vector-LPX treated groups to exclusively evaluate the oncotoxicity of NS1 and not the unspecific effects of cationic lipid components (Fig. S5). A strong decrease in cell viability due to NS1 expression was found in some cell lines (*e.g.* Hep3B), whereas others did not respond to a NS1-LPX treatment (*e.g.* Sk-Hep1), as shown in Fig. 3A. No correlation between oncotoxic effects of NS1 and cytotoxicity of empty LPXs was observed (Fig. S5). Importantly, freshly isolated PHH were only weakly affected

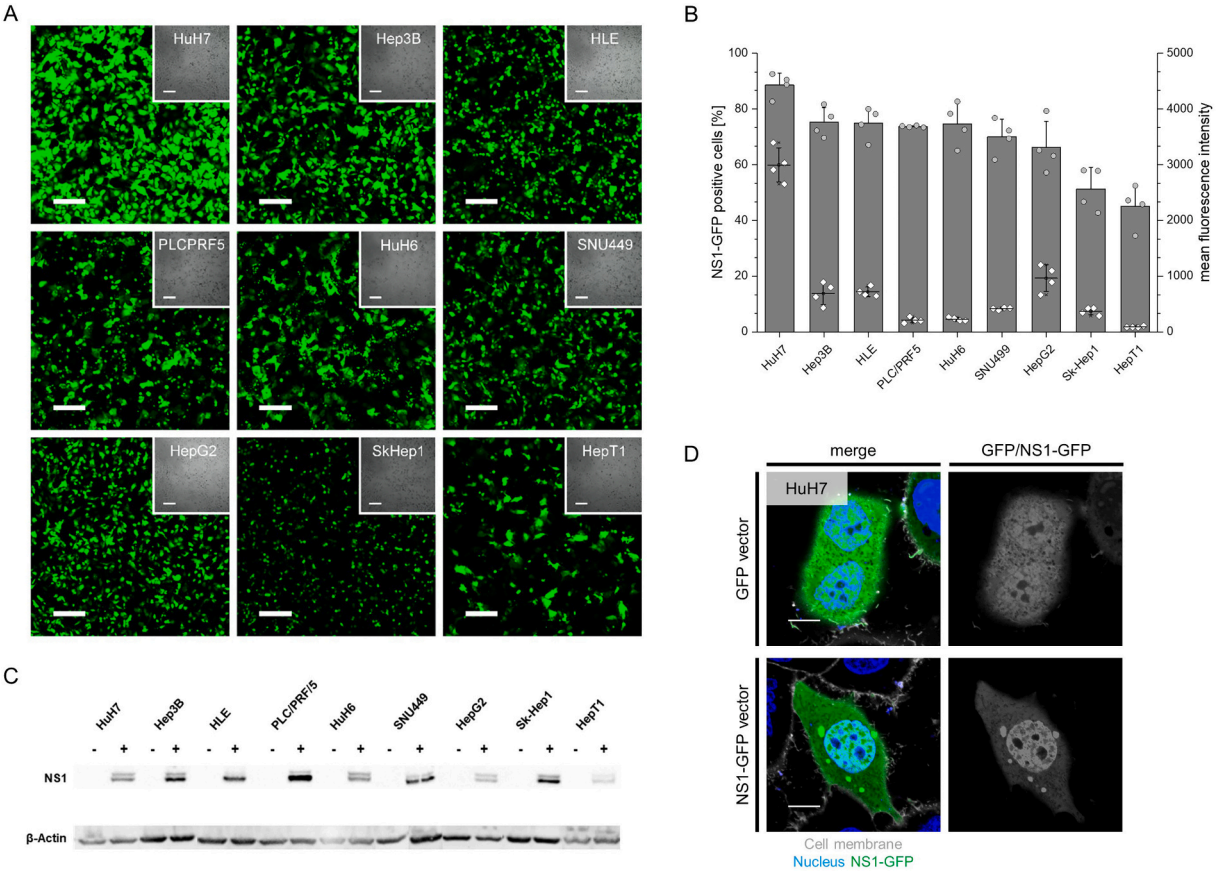

Fig. 2. NS1-LPXs efficiently deliver NS1 *in vitro*. **A**, NS1-GFP-LPX delivery and expression of NS1-GFP by human liver cancer-derived cell lines. Confocal microscopy and bright field (insert) images taken after 24 h. Scale bar, 150 μm. **B**, Quantitative analysis of NS1-GFP in human liver cancer-derived cell lines by flow cytometry 24 h after LPX-based gene delivery. Means ± S.D. of percentage of NS1-GFP positive cells (grey bars) and respective mean fluorescence intensities (white diamonds). $N = 4$. **C**, NS1-LPX transfection (+) results in expression of NS1 protein in human liver cancer-derived cell lines. Isolated bands of a representative western blot are shown. Complete images of the same blots are provided in *Supplemental Information*, Fig. S2. **D**, Confocal microscopy analysis of transfected HuH7 cells expressing GFP or NS1-GFP 4 h after NS1-GFP-LPX delivery. Left panel: overlay of fluorescence signals. Right panel: GFP signals reveal subcellular accumulation of NS1-GFP within cell nuclei (except nucleoli). Scale bar, 10 μm.

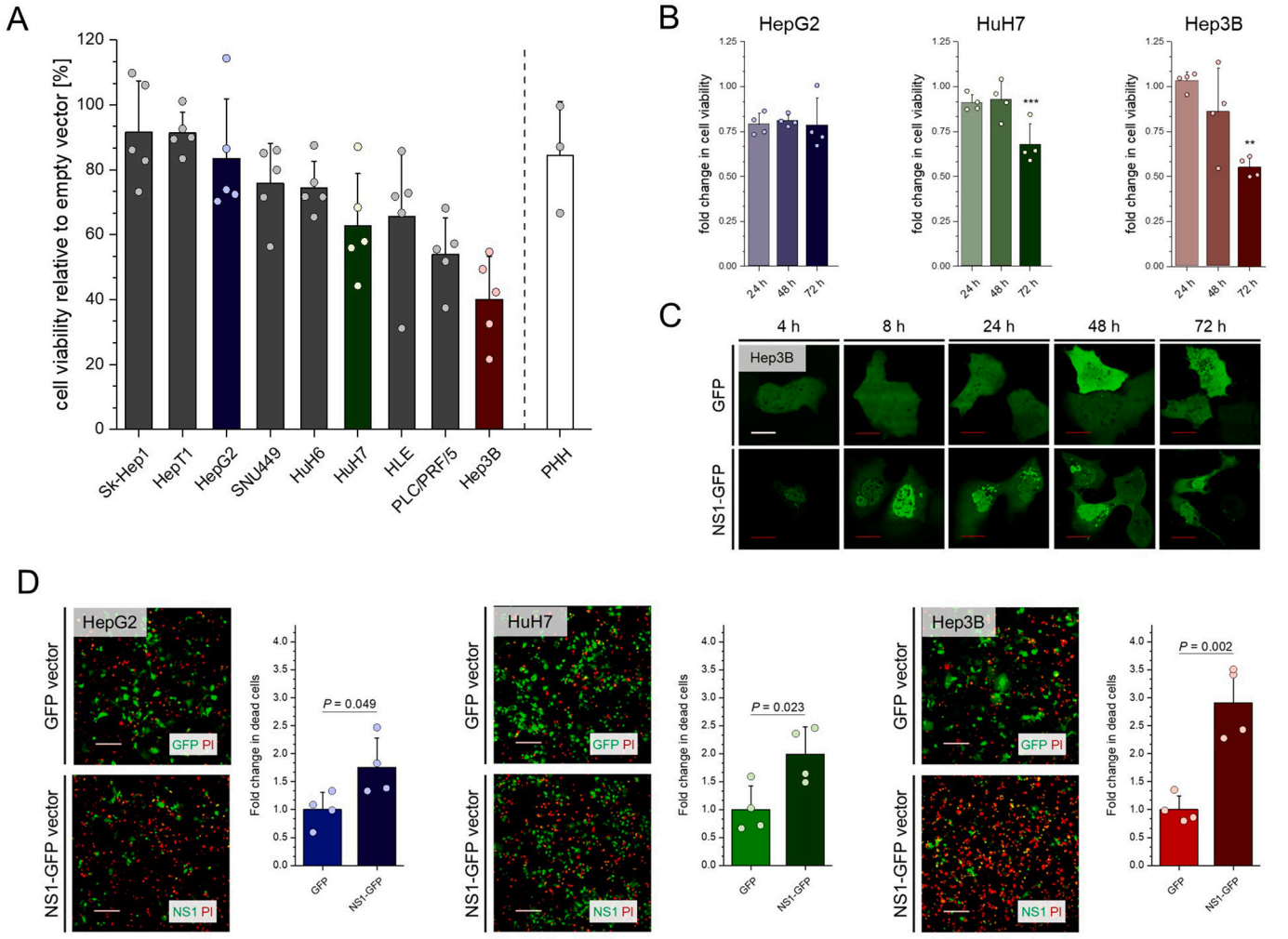

Fig. 3. NS1-LPXs selectively induce cell death in human liver cancer cells. **A**, NS1-LPXs reduce cell viability in human liver cancer cells. Cell viability (MTT assay) 72 h after NS1-LPX transfection. Control: transfected primary human hepatocytes (PHH). Means ± S.D. $N = 5$. **B**, Decrease in cell viability is cell type- and time-dependent. Control: empty vector-LPX treated cells defined as 1.00 viability. Means ± S.D. $N = 4$. **C**, Time-dependent alterations in cell morphology in NS1-GFP-LPX transfected Hep3B cells. Scale bar, 20 μm. **D**, NS1-LPXs induce cell death. Confocal microscopy images of propidium iodide (PI, red color) stained cells 72 h after GFP- or NS1-GFP-LPX treatment. Quantitative image analysis: Means ± S.D. $N = 4$. Statistical analysis was performed using one-way ANOVA with a Bonferroni *post hoc* test. *** $P < 0.001$, ** $P < 0.01$, * $P < 0.05$ *vs.* empty vector-LPX treated cells. (For interpretation of the references to color in this figure legend, the reader is referred to the web version of this article.)

by cationic LPXs and the expression of NS1 highlighting the potential of a NS1-LPX-based therapy to selectively kill malignant cells (Fig. 3A and Fig. S6). With respect to LPX uptake or NS1 expression (CMV promoter), NS1-LPXs do not show a selectivity towards tumor cells. However, DNA vectors can enter the nucleus only during G2/M mitotic phase of dividing cells due to a temporarily compromised nuclear membrane [34]. Since PHH divide with doubling times of months, translocation of DNA from the cytoplasm into the nucleus is a major limiting barrier. A facilitated gene expression in tumor cells as compared to healthy cells is therefore expected. No correlation between LPX uptake or NS1 expression and therapeutic response was observed within our panel of human liver cancer-derived cell lines (Fig. S7). Thus, a weakly (HepG2), a medium (HuH7), and a strongly responsive cell line (Hep3B) were selected to analyze the kinetics and mechanisms of NS1-induced cell death after LPX delivery. The varying responsiveness of these liver cancer-derived cell lines to NS1 is supported by data from literature [35]. A time-dependent decrease of cell viability was observed for Hep3B and HuH7 cells whereas HepG2 cells showed a constant viability over 72 h (Fig. 3B). In line with these results, responsive cell lines treated with NS1-GFP-LPXs showed strong morphological alterations over time, whereas cell morphology of control cells treated with GFP-LPXs showed no alterations over 72 h (Fig. 3C and Fig. S8). It can thus be concluded that NS1 activity is preserved despite fusion to the N-terminus of GFP. Results are in agreement with previous reports of the PV minute virus of mice (MVM) NS1, demonstrating deleterious effects to the cytoskeleton through NS1 interference with the regulation of actin/tropomyosin dynamics [17,20,36,37]. The membrane integrity of treated cells was then assessed by propidium iodide (PI)-staining (Fig. 3D) and intracellular ATP levels were determined (Fig. 4A) to investigate cell death through necrosis and/or apoptosis after treatment with GFP- or NS1-GFP-LPXs. Whereas weakly responsive HepG2 cells showed a small albeit statistically significant increase in cell death after NS1-GFP-LPX treatment (1.75× fold, $P = 0.049$), NS1 treatment of Hep3B cells resulted in a significant threefold increase in dead cells ($P = 0.002$). All three cell lines showed decreased intracellular ATP levels after treatment with NS1-LPXs indicating reduced metabolic activity (Fig. 4A). Here again, strongest effects were observed in Hep3B cells. These cells showed a significant increase in apoptosis and in necrosis over time (at reduced LPX concentrations), whereas effects in HuH7 and HepG2 cells treated with NS1-LPXs were comparable to a treatment with empty vector-LPXs (Fig. 4B and C). Since NS1 was shown to modulate heterologous promoters, a next generation RNA sequencing analysis of

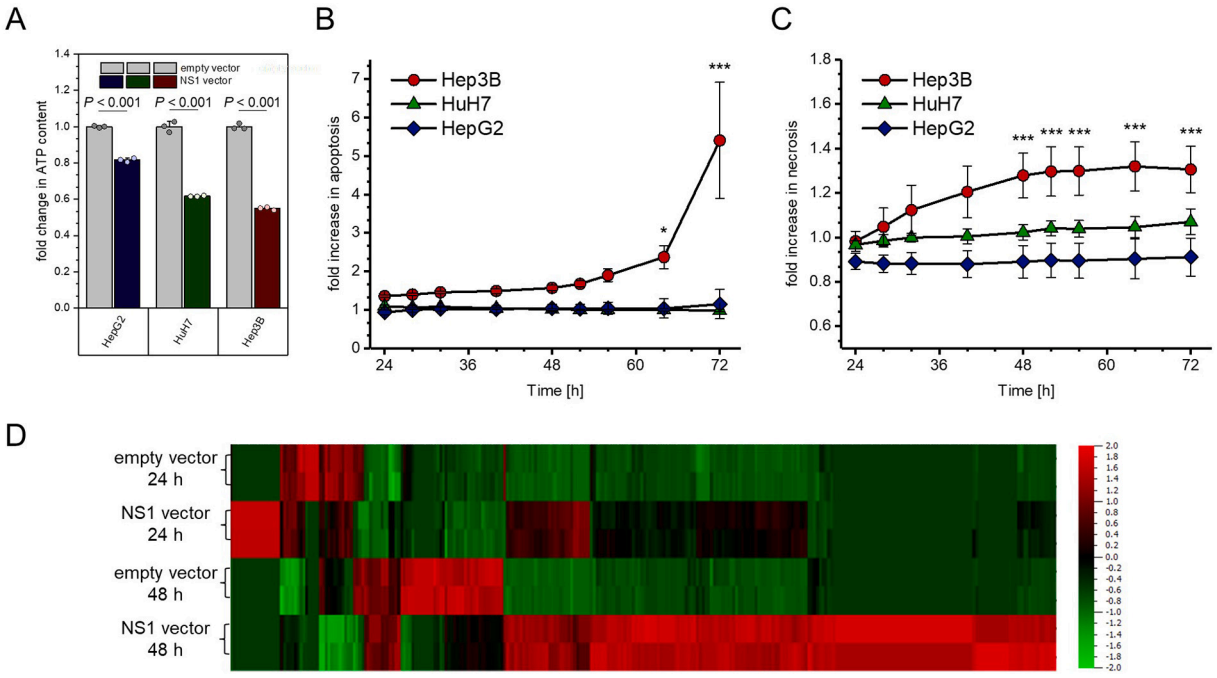

Fig. 4. NS1-LPXs disrupt cell metabolism and alter gene expression. **A**, NS1-LPXs induce reduction of intracellular ATP levels 72 h post transfection in liver cancer cells as compared to control (empty vector-LPXs). Means ± S.D. $N = 3$. **B**, NS1-LPXs induce apoptosis in a time-dependent manner (reduced LPX concentration) analyzed by RealTime-Glo™ assay. Means ± S.D. $N = 3$. **G**, NS1-LPXs induce necrosis (RealTime-Glo™ assay). Control: empty vector-LPX treated cells. Means ± S.D. $N = 3$. Statistical analysis of **A, B,** and **C** was performed using one-way ANOVA with a Bonferroni *post hoc* test. *** $P < 0.001$, ** $P < 0.01$, * $P < 0.05$ *vs.* empty vector-LPX treated cells. **D**, NS1-LPXs induce a change in gene expression in Hep3B cells as compared to empty vector-LPXs. RNA-seq data at indicated time-points. $N = 2$. Hierarchical clustering of samples based on differentially expressed genes (normalized fold-change −2.0 to 2.0, false discovery rate at $P < 0.05$) highlights major changes in gene expression patterns. Details on differentially expressed genes are provided in *Supplemental Information*, Fig. S9 and S10.

Hep3B cells after treatment with NS1-LPXs was performed to identify NS1-induced death pathways [38]. Indeed, treatment with NS1-LPXs revealed changes in global gene expression patterns as compared to cells treated with empty vector-LPXs (Fig. 4D, Fig. S9 and S10 and Table S2). Upregulation of gene expression post NS1-LPX treatment, including *DUOXA2, IL-4*, and *GAS7*, are indicative of ROS production, apoptotic events, and growth inhibition, respectively. An ingenuity pathway analysis was performed to cluster differently expressed genes with their molecular and cellular functions. Differences in gene expression after NS1-LPX treatment were associated with cell-cell signaling, cell morphology, cellular development, cellular growth and proliferation (Table S3). These changes in gene expression could be a consequence of NS1-LPX mediated cytotoxic effects or could be directly induced by NS1 as described in previous studies [38–41]. NS1 is capable to interfere with cellular transcription through several complementary mechanisms such as direct promoter interaction, interaction with cellular transcription factors, or by modifying the transcription machinery.

2.3. NS1-LPXs induce multimodal cell death

Interestingly, recent work has demonstrated that H-1PV infection induces multimodal cell death in various types of cancer [36,41–43]. In line with these findings, both apoptosis and necrosis contributed to NS1-LPX induced cell death (see kinetic assay results in Fig. 4B and C). Therefore, it was analyzed whether NS1-LPX treatment is also able to induce such multimodal cytotoxic effects in liver cancer cells (Fig. 5A). A complementary array of methods was used to further investigate molecular mechanisms of the NS1-LPX treatment. First, cells treated for 72 h with NS1-LPXs were analyzed after Annexin V/PI staining by flow cytometry to enable highly sensitive single-cell analysis (Fig. 5B). For all *in vitro* experiments, 0.1 ng pDNA/cell was used. NS1-LPX treatment significantly induced apoptosis in Hep3B (29.6 ± 1.8% of total cells, $P < 0.001$) and HuH7 (12.2 ± 3.0% of total cells, $P = 0.016$) cells, whereas the fraction of apoptotic cells in weakly responsive HepG2 cells was comparable to empty vector-LPX treatment (Fig. 5B). Furthermore, the relative increase in necrosis in NS1-LPX treated cells as compared to empty vector-LPX treated cells was higher in Hep3B as compared to HuH7 or HepG2 cells (Fig. 5B). An increase in cleaved forms of caspase 9, caspase 3, and PARP in Hep3B and HuH7 cells were observed, indicating induction of apoptosis, 48 h and 72 h after NS1-LPX uptake (Fig. 5C and D). In line with these results, enzymatic activity of effector caspases 3 and 7 significantly increased over time in Hep3B ($P < 0.001$) and HuH7 ($P < 0.05$) cells after NS1-LPX treatment (Fig. 5E). No difference between NS1- and empty vector-LPX treatment was observed in weakly responsive HepG2 cells (Fig. 5E). Recent studies showed that accumulation of reactive oxygen species is a major mechanism for NS1-mediated apoptosis after H-1PV or PV MVM infection [43]. A fluorescence-based technique was used to qualitatively and quantitatively (Fig. 6A and B) detect intracellular superoxide levels exclusively induced by NS1 expression (not viral infection). NS1-GFP-LPX treatment resulted in increased intracellular superoxide levels (Fig. 6A). Interestingly, gating for NS1-GFP positive cells revealed that elevated superoxide levels were specific for NS1-GFP expressing cells ($P = 0.005$) whereas NS1-GFP negative cells or LPX-GFP treated cells showed unaffected superoxide levels as compared to empty vector-LPX treatment (Fig. 6B). This effect was associated with increased DNA fragmentation (Gel DNA smear/fragmentation) and increased DNA damage response, indicated by elevated levels of gamma histone 2AX (Fig. 6C and Fig. S11). In agreement with previous reports with PV MVM, it can be concluded that NS1-LPX treatment of liver cancer cells results in a sequence of multiple events, *e.g.* superoxide induction and phosphorylation of histone 2AX within 24 h, DNA damage, ATP depletion, and mitochondrial stress after 24 h, initiation of caspase signaling within 24–48 h, and apoptosis and necrosis after 48 h [44,45].

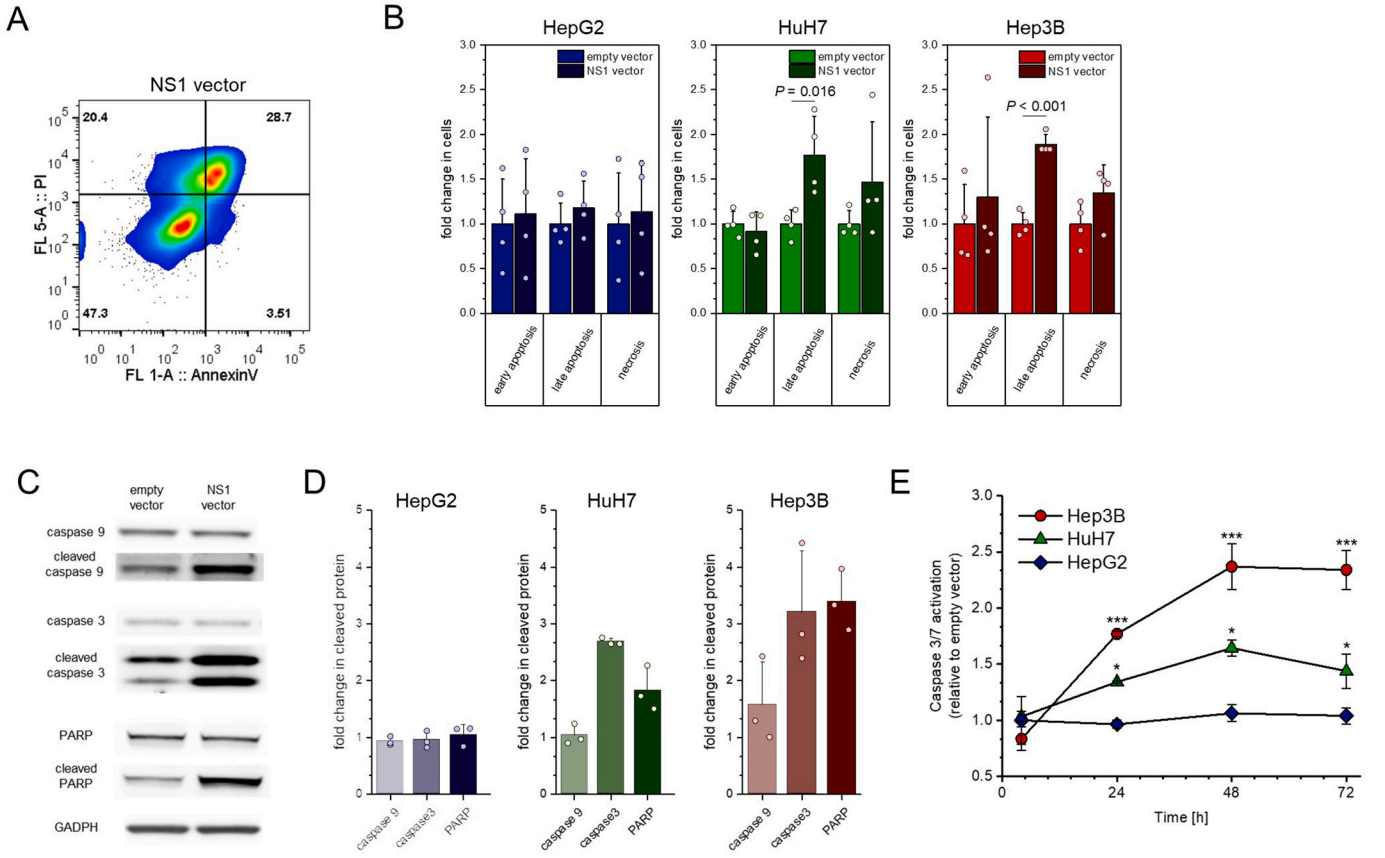

Fig. 5. NS1-LPXs induce multimodal cell death in liver cancer cells. **A**, Schematic overview of NS1-LPX induced multimodal cell death illustrating NS1 interference with target cell processes and their impact. **B**, Quantitative analysis of apoptosis and necrosis. Flow cytometry data are shown as percentage of total cells. Means ± S.D. $N = 4$. **C**, NS1-LPXs induce cleavage of pro-apoptotic caspases and PARP in Hep3B cells. A representative western blot 72 h after treatment is shown. **D**, Quantitative analysis of western blot images (panel c) of cleaved caspase 9, caspase 3, and PARP 72 h after NS1-LPX treatment. Fold change as compared to empty vector-LPX treated cells. Means ± S.D. $N = 3$. **E**, NS1-LPXs increase activity of effector caspases 3 and 7 in a cell type- and time-dependent manner. Means ± S.D. $N = 3$. Statistical analysis was performed using one-way ANOVA with a Bonferroni *post hoc* test. *** $P < 0.001$, ** $P < 0.01$, * $P < 0.05$ *vs.* empty vector-LPX treated cells.

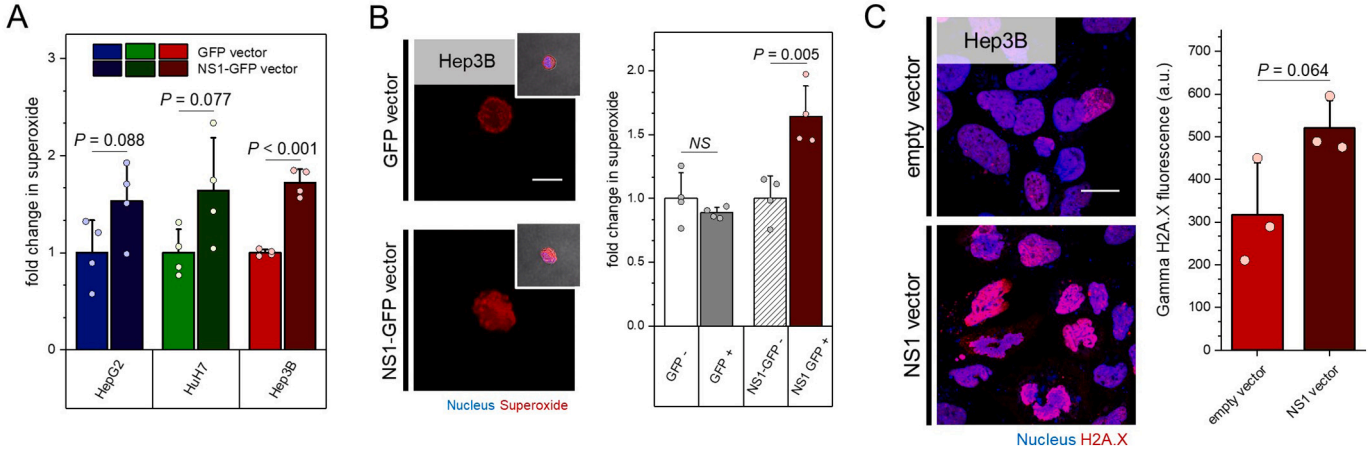

Fig. 6. NS1-LPXs induce oxygen stress in liver cancer cells. **A**, NS1-GFP-LPXs induce superoxide accumulation 24 h after GFP-LPX (control) or NS1-GFP-LPX treatment. Fold change as compared to control. Means ± S.D. $N = 4$. **B**, NS1-LPXs induce intracellular accumulation of superoxide in Hep3B cells 24 h post transfection. Control: GFP-LPXs. Scale bar, 10 μm. Quantitative analysis by flow cytometry and gating based on GFP/NS1-GFP expression. Means ± S.D. $N = 4$. **C**, NS1-LPXs induce DNA damage 24 h post transfection based on increase of gamma histone 2AX (γ-H2AX) in cell nuclei. Control: empty vector-LPXs. Quantitative image analysis: Means ± S.D. $N = 3$. Statistical analysis was performed using one-way ANOVA with a Bonferroni *post hoc* test. *** $P < 0.001$, ** $P < 0.01$, * $P < 0.05$ *vs.* empty vector-LPX treated cells.

2.4. PDK1 is a suitable biomarker for patient stratification

Within our panel of nine human liver cancer-derived cell lines, we did not observe a correlation between gene delivery efficiency (*i.e.* LPX uptake, transfection efficiency, NS1 expression levels) and cytotoxic effects. Since the cellular response towards NS1 is limited to certain

neoplastic cells, the question arises whether predictive biomarkers can be identified, which can be used to identify NS1-responsive cells. This would allow patient stratification prior to therapy.

Subsequent experiments therefore focused on the intracellular activation pathway of NS1. It should be noted that NS1 acts like a prodrug that needs intracellular activation by phosphorylation to exert a pharmacological function. Several cell transformation dependent cellular factors and signaling cascades are linked to NS1 activation and toxicity [13,41]. Recently, it was revealed by our group that PDK1 signaling is a predictive marker for the efficacy of H-1PV in glioma therapy [29]. This results from a strong interplay between NS1, PDK1, and downstream kinases of the protein kinase C family (*e.g.* PKC isoform eta, PKCη), which acts in a loop-back mechanism to stimulate both, PDK1-dependent pathways (including PKB/Akt1) and NS1 - the latter through PKCλ and PKCη phosphorylation [14]. PKC isoforms were shown to interact with H-1PV NS1 *in vivo* resulting in nuclear colocalization [46,47]. A key element for this interplay appears to be the ERM-family protein radixin, which directly interacts with NS1 and PKCη, thereby modulating substrate specificity of this kinase [29,46–48]. It should be noted that the impact of H-1NS1 expression on normal human cells upon H-1PV infections has been studied previously. In particular, these studies revealed that H-1PV NS1 is not capable to activate the PDK-1 signaling cascade in normal human cells [29].

An overview of previously published phosphorylation sites of NS1 are provided in Fig. S12 [14]. T585 is a known target of PKCλ and is associated with toxic functions of NS1. To investigate whether response to NS1-LPXs was dependent on endogenous PDK1 levels, PDK1 expression levels in the selected panel of liver cancer cells were analyzed by ELISA. Interestingly, a clear correlation between NS1-LPXs susceptibility and PDK1 levels was observed. Strongly responsive Hep3B cells had significantly higher PDK1 expression levels ($P = 0.04$) as compared to weakly responsive HepG2 cells (Fig. 7A). Notably, alternative activation mechanisms of PDK1 (downstream) signaling might result in increased efficacy of NS1-LPX treatment besides elevated PDK1 levels. A constitutively activated PDK1 isoform (PDK1:S138E) was therefore overexpressed in these liver cancer cells using recombinant adeno-associated viruses [29]. Ectopic PDK1 expression resulted in a significant increase in NS1-LPX mediated cytotoxicity in weakly responsive HepG2 cells ($P < 0.001$) and medium responsive HuH7 cells ($P < 0.004$) as compared to empty vector-LPX treated cells (Fig. 7B and Fig. S13). No further increase in cell death was observed for strongly responsive Hep3B cells, indicating that endogenously elevated PDK1 expression levels are sufficient for maximal NS1-LPX-mediated cytotoxicity (Fig. 7B). Next, the intracellular localization of PDK1 downstream kinases was analyzed. PKCη significantly colocalized with NS1 in cell nuclei in Hep3B cells ($P < 0.001$) whereas increased nuclear accumulation of PKCη was only minor in HepG2 and HuH7 cells after NS1-LPX treatment (Fig. 7C and Fig. S14). Expression of PDK1 in tissue samples from HCC patients was then analyzed using RNA and tissue microarrays. PDK1 mRNA levels were significantly increased in tumoral areas as compared to non-tumoral areas in HCC patients ($P = 0.0027$) (Fig. 8A and Fig. S15). These findings were confirmed on a protein level. PDK1 staining

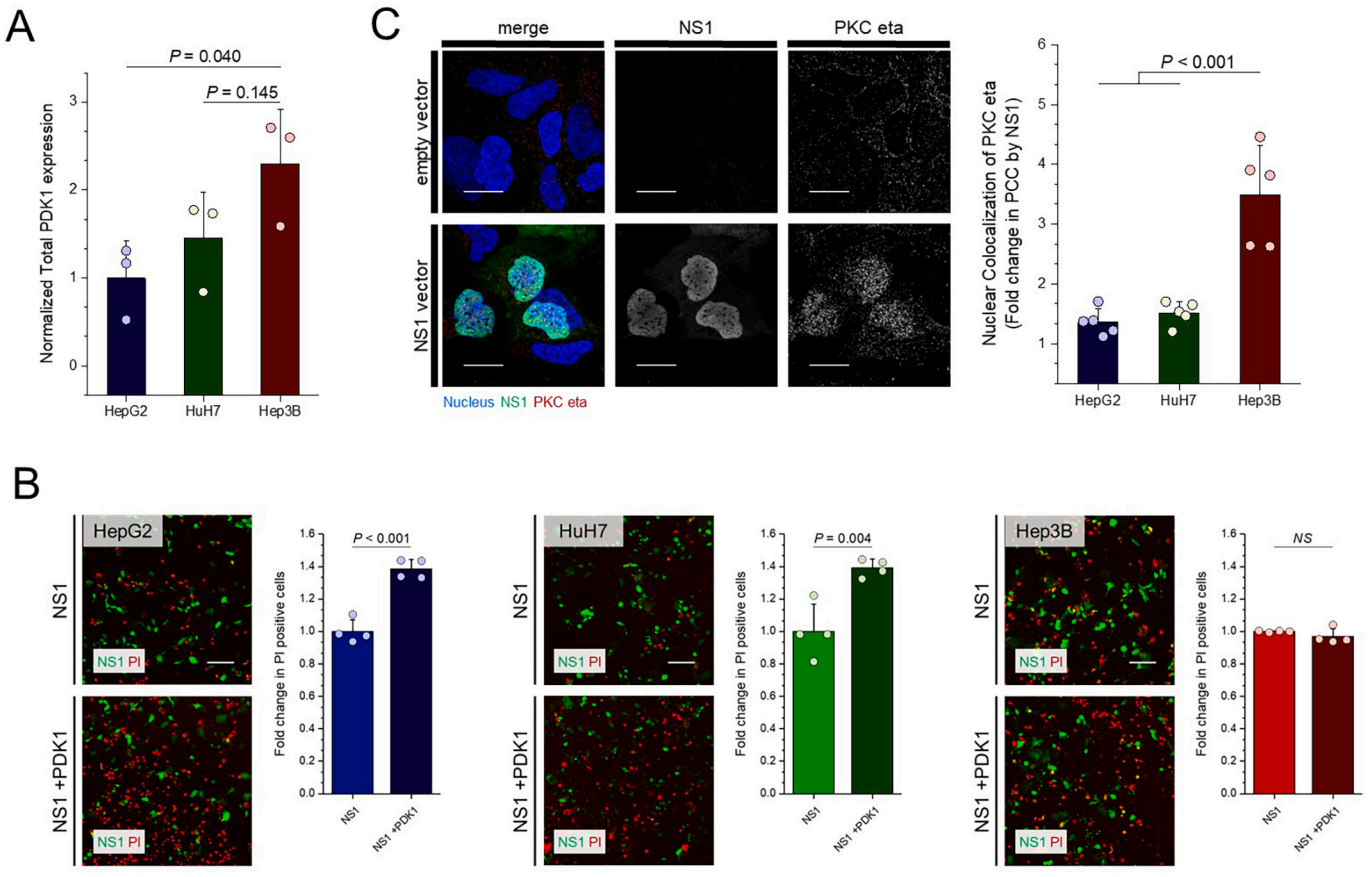

Fig. 7. Phosphoinositide-dependent kinase 1 (PDK1) as a marker for susceptibility to NS1-LPX treatment. **A**, Total PDK1 in liver cancer-derived cell lines based on ELISA. PDK1 signals were normalized to total protein. Means ± S.D. $N = 3$. **B**, Overexpression of constitutively active PDK1 (PDK1:S138E transduction) renders weakly responsive HepG2 and HuH7 cells susceptible for NS1-LPX therapy. Dead cells are stained by propidium iodide (PI, red color) 72 h after GFP-LPX (control) or NS1-GFP-LPX treatment. Representative confocal microscopy images are shown. Scale bar, 25 μm. Quantitative image analysis: Means ± S.D. $N = 4$. **C**, PKC isoform eta colocalization with NS1 24 h after NS1-LPX treatment. Representative confocal microscopy images of Hep3B cells are shown. Scale bar, 10 μm. Pearson's colocalization correlation (PCC) analysis. Means ± S.D. $N = 5$. Statistical analysis of **A**, **B**, and **C** was performed by one-way ANOVA with a Bonferroni *post hoc* test. (For interpretation of the references to color in this figure legend, the reader is referred to the web version of this article.)

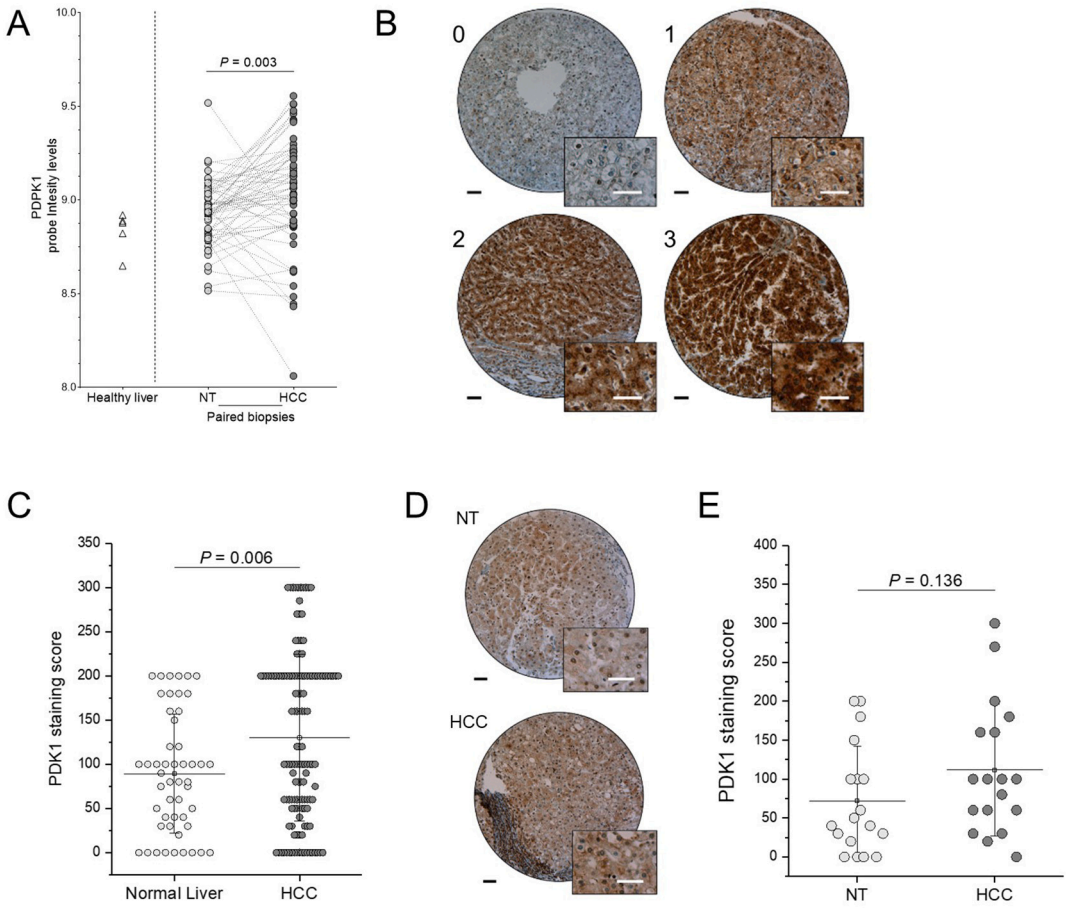

Fig. 8. Phosphoinositide-dependent kinase 1 (PDK1) expression in human HCC patients. **A**, Elevated *PDK1* mRNA levels in tumor areas of human HCC biopsies. *PDK1* RNA microarray of $N = 64$ patient samples. Control: healthy liver or non-tumoral tissue. **B**, Immunohistochemical PDK1 protein expression analysis in human tissue samples (normal liver or HCC). Classification based on PDK1 staining scores 0–3. **C**, Elevated PDK1 protein levels in HCC as compared to healthy liver. Means ± S.D. $N = 183$ patient samples. **D**, Representative tissue microarray punches of non-tumoral and HCC tissue in a patient with HCC. Scale bar, 50 μm. **E**, PDK1 staining scores from non-tumoral and tumoral matched liver specimen in patients with T1/T2 HCC stage. Means ± S.D. $N = 18$ patients. Statistical analysis of **A**, **C**, and **E** was performed by one-way ANOVA with a Bonferroni *post hoc* test.

intensity and area were categorized in PDK1 scores 0–3 (Fig. 8B). PDK1 expression was significantly higher in HCC specimen as compared to healthy liver ($P = 0.006$) tissue (Fig. 8C and Table S4-S6). Furthermore, PDK1 scores were higher in tumoral areas as compared to non-tumoral areas in matched biopsies (Fig. 8D and E, Fig. S16 and Table S7). In summary, PDK1 expression levels correlate with NS1-LPX susceptibility (*i.e.* increased cytotoxic effects with increasing PDK1 levels). PDK1 is therefore a valuable marker for patient stratification. Elevated PDK1 is proposed to be a prerequisite for NS1 based cancer nanomedicines [49]. Patients with elevated PDK1 levels in HCC tissue can be selected for a NS1-LPX-based tumor treatment. The present results demonstrate that around 10% of HCC patient would fulfil the stratification criteria for a NS1-LPX-based therapy (PDK1 Staining Score 3: tumoral 11.1% *vs.* non-tumoral 0.0%).

2.5. NS1-LPXs reduce HCC tumor growth and extend survival in vivo

Data shown above indicate that LPX mediated H-1PV NS1 expression induces a cytotoxic response in human tumor cells. As proof-of-concept to demonstrate the therapeutic potential of NS1, a first-in-rodent study for intratumorally (*i.t.*) administered NS1-LPXs in mice carrying Hep3B xenografts (*i.e.* subcutaneous human solid tumors) was performed. It should be noted that cell killing is not specific for transformed human cell lines. Mouse cells resist H-1PV infection due to restrictions during cell entry. This limitation can be circumvented through pseudotyping with MVM capsids [12]. Upon transfection, however, both NS1 species appear to exert toxicity to cancer cell (-lines) of heterologous origins. Indeed, transfection experiments of H-1PV and MVM NS1 sequences in mouse A9 cells and human glioma NCH149 cells demonstrate toxicity of the respective highly homologous proteins as compared to non-toxic GFP (Supplementary Fig. S19). It can be concluded that, in contrast to infections with H-1PV, mouse model systems are suitable to monitor off-target effects of transduced non-murine PV NS1 proteins. Local administration of NS1-LPXs was selected as administration route to maximize the direct exposure of cancer tissue while minimizing distribution to non-target organs. It should be noted that intravenous injection of cationic nanoparticles would result in first-pass filtration in the lung, and thus, rapid clearance from circulation [27,50]. Therefore, LPXs used in this study were *i.t.* administered, which is a well-established intervention for several gene therapies in a clinical setting [51–53]. Within cancer tissue, the positive surface charge of LPXs mediates interactions with tumor cells and thereby increases transfection efficacy. Mice were randomized ($N = 6$ per group) and empty vector- or NS1-LPXs were injected *i.t.* with a dosing interval of 5 days for one month (*i.e.* 7 injections) as outlined in Fig. 9A. No changes in behavior or body weight were observed during therapy with both LPX formulations (Fig. S17).

Treatment with NS1-LPXs significantly ($P = 0.0086$) reduced tumor growth (Fig. 9B) and reduced the absolute tumor volume (Fig. 9C and Fig. S18). Furthermore, NS1-LPX treatment prolonged the mean survival of mice from 29 to 40 days. NS1 expression in Hep3B tumors was

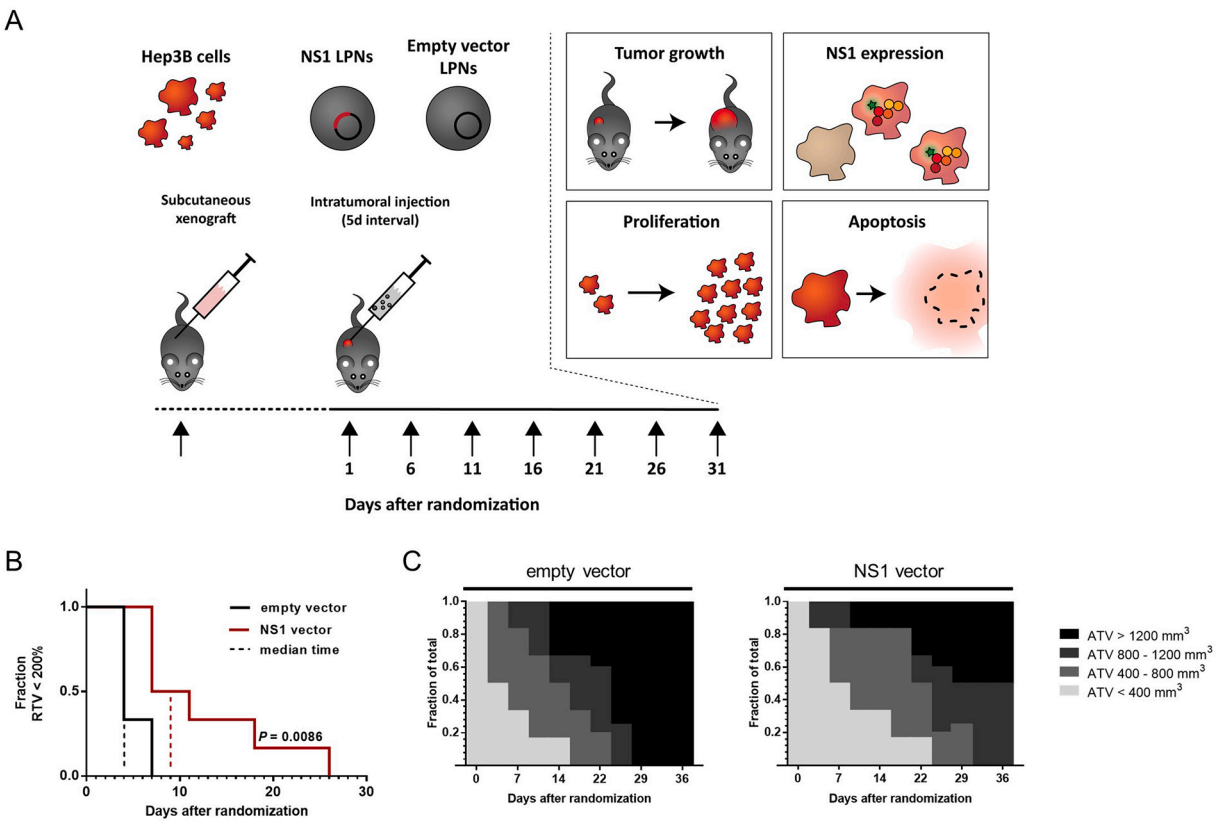

Fig. 9. Reduced tumor growth in a Hep3B xenograft mouse model *in vivo* after NS1-LPX transfection. **A**, Empty vector- or NS1-LPXs were administered at a dosing interval of 5 days by repeated intratumoral injections. **B**, Kaplan Meier analysis of mice treated with empty vector- or NS1-LPXs based on doubling of initial tumor volume. Start: 100% = 150 mm^3. Endpoint was defined as relative tumor volume (RTV) $\geq$ 200%. Dashed lines indicate median time to reach endpoint. **C**, NS1-LPXs reduce tumor growth as compared to empty vector-LPX treated mice. Bin analysis of absolute tumor volumes (ATV in mm^3). Results are shown as fraction of total number of mice. $N = 6$ animals per treatment group. One animal in the empty vector-LPX treated group was excluded for mRNA and protein analysis due to ulceration at tumor site. Statistical analysis of **B** was performed by Gehan-Breslow-Wilcoxon test.

analyzed by RT-PCR (Fig. 10A) and immuno-fluorescence (Fig. 10B). Three out of 6 animals treated with NS1-LPXs showed high NS1 protein expression levels (Fig. 10B). Interestingly, NS1 protein expression significantly correlated inversely ($R = -0.925$, $P = 0.008$) with the last observed absolute tumor volume during therapy (Fig. 10C). Less proliferating (*i.e.* Ki67 positive) cells were found in tumors treated with NS1-LPXs as compared to tumors isolated from empty vector-LPX treated mice ($P = 0.245$) as indicated in Fig. 10D. Since apoptosis was a major contributor to therapeutic effects observed *in vitro*, tumor samples were stained for cleaved caspase 3 to detect apoptotic activity (Fig. 10E). Increased levels ($P = 0.119$) of cleaved caspase 3 were found in immunohistochemistry staining of NS1-LPX treated tumors (Fig. 10E) confirming an apoptotic cell death induction by NS1 *in vivo*. Further advances in lipid nanoparticle technology and improvement in nucleic acid design are needed to increased potency and to extend dose intervals [27]. In a clinical setting, *i.t.* deposition of NS1-LPXs (*i.e. via* computed tomography-guided *i.t.* injection or hepatic catheterization) could be used for the treatment of HCC since chemoembolization of HCC *via* hepatic catheters is already routine practice and similar concepts for gene delivery to other organs such as the heart were already exploited [54–57]. Questions related to immunogenicity upon H-1PV infection were studied previously by Morales et al. [58] as well as in clinical studies with glioma patients treated with H-1PV [22].

3. Conclusion

Data presented in this study provide first evidence that intracellular expression of the cytotoxic protein NS1 is a promising strategy to selectively treat HCC with elevated PDK1 levels. Mechanistic studies *in vitro* demonstrated the interaction with host cell kinases. Superoxide production followed by DNA damage and activation of pro-apoptotic proteins significantly induced cell death in malignant cells. This therapeutic strategy resulted in reduced tumor growth and prolonged survival in a mouse xenograft tumor model. To date, no treatment options are available for HCC besides the multi-tyrosine kinase inhibitors sorafenib, regorafenib and lenvatinib, which have shown a consistent (10 to 12 weeks) prolonged survival. However, limited increase in patient survival and emerging resistance still result in poor clinical outcomes. The present findings may extend the therapeutic options for the treatment of HCC using non-viral gene delivery systems to express large anticancer proteins with tumor-cell specificity.

4. Experimental section

4.1. Experimental details

4.1.1. Cloning of plasmids

pcDNA3.1$^+$ was obtained from Invitrogen and pTagGFP-N was purchased from Evrogen. pdB-H-1PVwt (German Cancer Research Center DKFZ, Heidelberg, Germany) was used as template for NS1 gene amplification by polymerase chain reaction (PCR) using primers 1 and 2 (pcDNA3.1-NS1) and primers 1 and 3 (pTag-NS1-GFP). Phusion® High-Fidelity DNA Polymerase (New England Biolabs) was used according to the manufacturer's recommendation. DNA was initially denaturated at 98 °C for 30 s followed by 35 cycles of denaturating (98 °C, 10 s), annealing (67 °C, 30 s), and elongation (72 °C, 45 s). DNA was extended finally at 72 °C for 10 min. Subsequently, the PCR product was digested and ligated into the expression plasmids pcDNA3.1$^+$ (pcDNA3.1-NS1

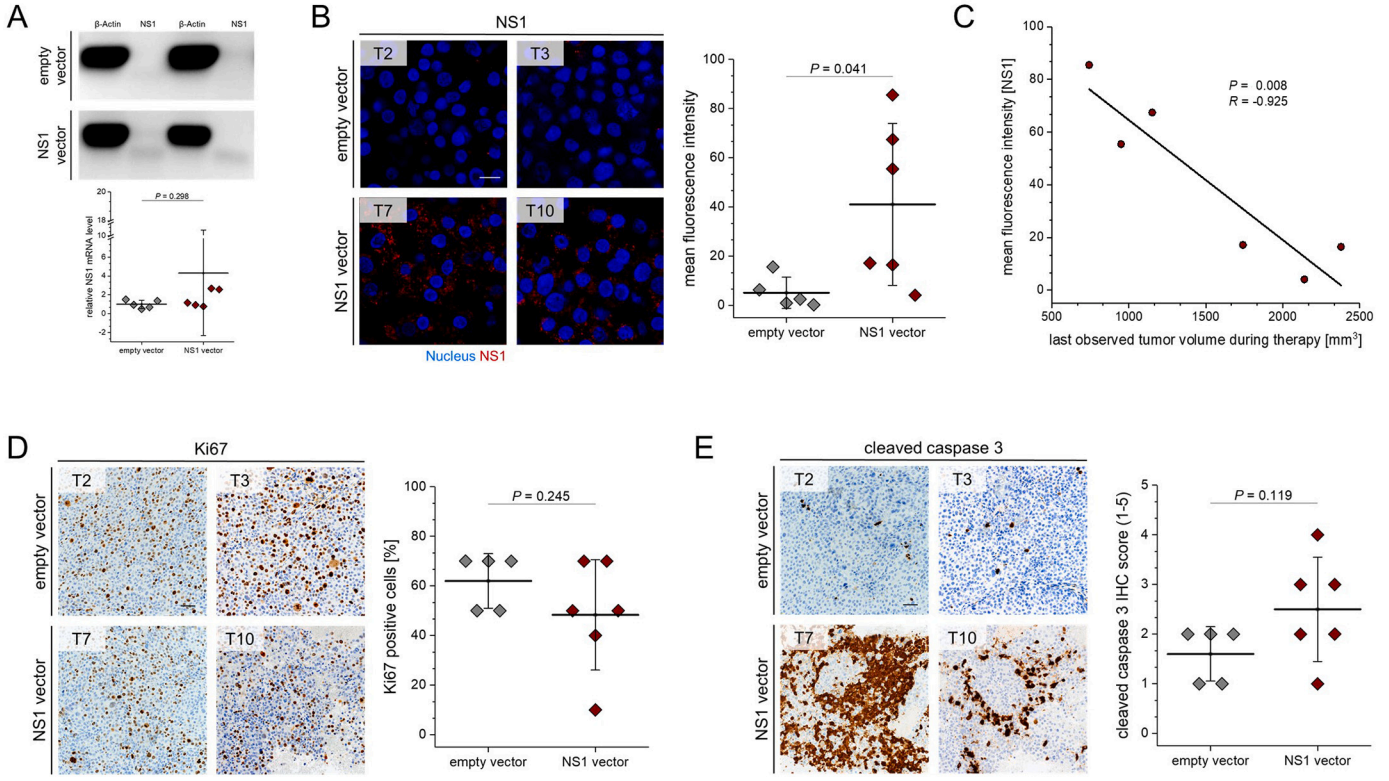

Fig. 10. NS1 is expressed in a Hep3B xenograft mouse model *in vivo* after NS1-LPX transfection and induces apoptosis. **A**, NS1 gene transcription in tumor cells. Representative PCR of *NS1* mRNA levels in tumors from mice treated with empty vector- or NS1-LPXs. Quantitative analysis: Means ± S.D. Reference: mRNA of *β-Actin* housekeeping gene. **B**, NS1 protein is expressed in NS1-LPX treated tumors. Representative confocal microscopy images after NS1 immunofluorescence staining are shown. Quantitative image analysis: Means ± S.D. **C**, Correlation of NS1 protein expression levels and last observed tumor volumes during therapy in NS1-LPX treated tumors. **D**, NS1-LPX treatment reduces cell proliferation in tumors as compared to empty vector-LPX treatment. Representative immunohistochemistry (IHC) images of tumors (T2, T3, T7, T10) stained for the proliferation marker Ki67 are shown. Percentage of Ki67 positive cells are shown as means ± S.D. **E**, NS1-LPX treated tumors show increased levels of activated caspase 3. Representative IHC images of tumors (T2, T3, T7, T10) stained for cleaved caspase 3 are shown. Cleaved caspase 3 IHC scores: Means ± S.D. $N = 6$ animals per treatment group. One animal in the empty vector-LPX treated group was excluded for mRNA and protein analysis due to ulceration at tumor site. Statistical analysis was performed by one-way ANOVA with a Bonferroni *post hoc* test. **C**, Pearson's r and R-Square is given for multi-data linear fit.

using BamHI and *Not*I sites) or pTagGFP-N (pTag-NS1-GFP using BamHI sites). The resulting plasmids were sequenced to confirm NS1 sequence and correct reading frame. The following primers were used for cloning, (1) 5′-attggatccgcgatggctggaaacgcttactcc-3′, (2) 5′-tattaatgcggccgct-tagtccaaggtcagctcctcg-3′, (3) 5′-aatggatccgcgtccaaggtcagctcctcg-3′. Plasmids that were used for lipoplexes (LPX) preparation were purified using the QIAprep Plasmid PlusMidi Kit (Qiagen) in accordance with the manufacturer's recommendations.

4.1.2. LPX preparation and characterization

LPXs used in this study were composed of a proprietary lipid mix (Lipofectamine 3000 transfection kit, Invitrogen) and plasmid DNA (pDNA) was complexed at an LPX:pDNA ratio of 2 (*V/w*). In brief, pDNA was diluted in OptiMEM (Gibco) mixed thoroughly, and P3000 reagent was added. Lipofectamine 3000 was diluted with OptiMEM, mixed with the pDNA mixture, vortexed, and incubated for 5 min at room temperature. For *in vivo* experiments, OptiMEM transfection medium was replaced by sterile glucose solution (5% *w/V*). N/P ratio was optimized to reach maximum gene delivery efficiency with minimum toxicity (data not shown).

4.1.3. Nanoparticle tracking analysis (NTA)

LPX size and size distribution was determined by NTA using a Nanosight NS200, LM20 (Malvern Instruments Ltd) equipped with a 405 nm laser as described previously [59]. In brief, the optical chamber was cleaned before measurements using 0.2 μm filtered water and absence of particles was confirmed. LPXs were injected using a 1 mL sterile syringe and videos of 90 s were recorded. NTA 2.2 software was used for capturing and analysis of average particle size and size distribution. A minimum of 300 completed tracks was analyzed to obtain statistically relevant data. Results are shown as means ± S.D. of $n = 3$ experiments.

4.1.4. Zeta potential measurement

The zeta potential of LPXs was determined using the Delsa Nano C Particle Analyser (Beckman Coulter). Samples were analyzed according to the Smoluchowski equation using a laser wavelength of 685 nm and a detection angle of 15° and converted. Results are shown as means ± S.D. of $n = 3$ experiments.

4.1.5. Transmission electron microscopy

LPXs were visualized by transmission electron microscopy (TEM) after negative staining. In brief, 5 μL of the LPX suspensions were mounted on a carbon-coated copper grid, negatively stained with uranyl acetate (2%), and dried overnight. Samples were then analyzed using a CM-100 transmission microscope (Philips) at an accelerating voltage of 80 kV. Average particle size was determined by measuring $n = 100$ particles.

4.1.6. Transfection of adherent cells using LPXs

A standard LPX transfection protocol was developed. Cells were seeded in complete cell culture medium at a density of 2.5×10^4 cells

per cm^2 onto poly-D-lysine coated (0.4 mg mL^{-1}) plastic cell culture plates (TPP), polymer bottom culture slides (μ-slide, Ibidi) or glass slides (Menzel Gläser) and allowed to adhere overnight. Freshly prepared LPX formulations were added to cells at a concentration of 1 μg mL^{-1} pDNA (*i.e.* 0.1 ng pDNA per cell).

4.1.7. NS1-LPX cellular uptake

Cellular uptake of LPXs by liver cancer-derived cell lines was analyzed by confocal microscopy. Cells were cultured as described on poly-D-lysine-coated polymer slides (μ-slide, Ibidi) and allowed to adhere overnight. LPXs encapsulating fluorescently labeled pDNA (DiYO-1, AAT Bioquest) were added and cells were incubated for indicated periods of time. Cells were then incubated with Hoechst 33342 (Sigma) at a final concentration of 0.1 μg mL^{-1} for 10 min at 37 °C and washed three times with D-PBS. Then, 200 μL of Cell Mask Deep Red Plasma Membrane staining solution (Thermo Scientific, 0.5 μL Cell Mask per 1 mL culture medium) was added. Cellular binding and internalization were visualized using an Olympus FV-1000 confocal microscope (Olympus) equipped with a 60× PlanApo N oil immersion objective (NA 1.42, Olympus). Images were processed using GIMP 2.8 software (GNU image manipulation program).

4.1.8. Confocal microscopy

NS1-GFP was analyzed by confocal microscopy. Cells were seeded in a 24-well plate and were transfected with GFP or NS1-GFP as described above. Expression of GFP and NS1-GFP was visualized using a FV1000 confocal microscope (Olympus) equipped with a 10× water immersion objective (NA 0.4, Olympus). Excitation and emission wavelength were 488 nm and 516 nm, respectively. For live cell imaging, cells were seeded on polymer bottom culture slides (μ-slide, Ibidi) and cultured in complete culture medium using phenol red-free DMEM (Gibco).

4.1.9. Flow cytometry

To quantify the percentage of NS1-GFP expressing cells and the average expression level, transfected cells were analyzed by flow cytometry. Cells were detached at indicated time points, washed once with D-PBS, centrifuged (400 xg, 5 min, 4 °C) and resuspended in FACS staining buffer (D-PBS supplemented with 0.05% NaN_3 and 1% FCS). Cells were then analyzed by flow cytometry using a FACS Canto II flow cytometer (Becton Dickinson) exciting at 488 nm. Doublets were excluded, and fluorescence signals were collected using FL1 (505LP-530/30 nm). Results were analyzed using Flow Jo VX (TreeStar) and percentage of NS1-GFP-positive cells was evaluated. Mean fluorescence intensities (MFI) were normalized to empty vector-LPX treated control cells. Results are shown as means ± S.D. of $n = 3$ experiments.

4.1.10. NS1 immunofluorescence staining and confocal microscopy

For analysis of NS1 expression in adherent cells, cells were seeded onto a 254 mm^2 glass cover slip (Menzel Gläser, #1.5) coated with poly-D-lysine (0.4 mg mL^{-1}). At indicated time points post transfection, cells were washed three times with D-PBS (0.5 mM Ca^{2+}, 1 mM Mg^{2+}) and fixed using 4% PFA (30 min, RT). Cells were then incubated with D-PBS (50 mM NH_4Cl) for 6 min at room temperature and permeabilized with Triton-X100 0.1% for 10 min at room temperature. Cells were washed three times with D-PBS (0.5 mM Ca^{2+}, 1 mM Mg^{2+}) and blocked with 10% FCS for 30 min. Cells were then incubated with a mouse monoclonal or rabbit polyclonal primary anti-NS1 antibody (JPF Nüesch, German Cancer Research Center DKFZ, Heidelberg, Germany) in FACS staining buffer for 2 h at room temperature. Cells were washed three times with D-PBS (0.5 mM -Ca^{2+}, 1 mM Mg^{2+}) and incubated with an Alexa488 labeled secondary antibody (Invitrogen, goat-anti-rabbit or donkey-anti-mouse, 1:500 dilution) in FACS staining buffer for 60 min at room temperature. Hoechst 33342 (Sigma) was added at a final concentration of 0.1 μg mL^{-1} for 10 min to visualize cell nuclei. Expression of NS1 was analyzed using a FV1000 confocal microscope (Olympus) using a 60× oil immersion objective (NA 1.42, Olympus). Emission wavelengths were 405 nm and 488 nm, fluorescence was detected at 425–575 nm and 500–545 nm, respectively.

4.1.11. Western blot analysis

Cells were seeded in 6 well plates (TPP) and transfected as described above. At indicated time points, cell culture medium was collected, and cells were detached in ice cold D-PBS using a pre-cooled cell scraper. Supernatant and cell suspension were pooled and centrifuged (590 xg, 5 min, 4 °C) and resuspended in lysis buffer (20 mM Hepes pH 7.5, 5 mM MgCl, 300 mM NaCl, 0.1% NP40) containing 1× protease and phosphatase inhibitor cocktail (Roche Diagnostics). Cells were incubated on ice for 30 min and vortexed every 10 min. Cell extracts were used immediately after preparation or snap frozen in liquid nitrogen and stored at −80 °C. Total protein concentration was determined using the Pierce BCA Protein Assay Kit (Thermo Scientific) according to the manufacturers' recommendation. For further analysis, samples were mixed with 4× Lämmli sample buffer (140 mM SDS, 20% glycerol, 25% β-mercaptoethanol, bromphenol blue) and incubated at 96 °C for 5 min. Equal amounts of total protein were separated by SDS-PAGE (7.5% acrylamide gels) at 120 V and subsequently transferred to PVDF membranes (GE Healthcare Life Sciences) using a semi-dry approach at 0.7 mA per cm^2 of membrane for 1.5 h. Membranes were blocked in 5% skim milk in TBS-T (20 mM Tris-HCl pH 7.5, 150 mM NaCl, 0.05% Tween 20) for 60 min at room temperature. Membranes were then incubated with a polyclonal primary anti-NS1 antibody (JPF Nüesch, German Cancer Research Center DKFZ, Heidelberg, Germany) over night at 4 °C in 5% skim milk in TBS-T, washed three times with TBS-T, and incubated with horseradish-peroxidase-conjugated secondary goat-anti-rabbit antibody (Bio-Rad) for 60 min at room temperature. Membranes were washed three times in TBS-T and proteins were detected using a ChemiDoc imaging system (Bio-Rad) after incubation with Pierce ECL Western Blotting Substrate (Thermo Scientific). Equal loading was confirmed by staining for beta actin (Santa Cruz). Cells treated with empty vector-LPXs were used as negative control.

4.1.12. Subcellular localization of NS1

To analyze expression and subcellular localization of NS1-GFP, cells were seeded in poly-D-lysine coated polymer bottom culture slides (μ-slide, Ibidi) and transfected as described above. At indicated timepoints, images were captured by confocal laser scanning microscopy (Ex: 488 nm, Em: 500–545 nm) using a FV1000 microscope (Olympus) equipped with a 60× oil immersion objective (NA 1.42, Olympus). Due to changes in NS1-GFP expression, laser intensity was adjusted at each time point. Cell nuclei and plasma membranes were stained 24 h post transfection using Hoechst 33342 (Sigma, Ex: 405 nm, Em: 425–575 nm) and Cell Mask Deep Red Plasma Membrane Stain (Thermo Scientific, Ex: 635 nm, Em: 655–755 nm), respectively (see NS1-LPX cellular uptake section).

4.1.13. Cell viability assay

In vitro cell viability was determined using the MTT assay. Cells were seeded in 250 μL of complete culture medium in poly-D-lysine coated 96-well plates (TPP). At indicated time points, 100 μL of the culture medium was removed and 100 μL of MTT working solution (Thiazolyl blue, 5 mg mL^{-1}) was added. Cells were incubated for 2–4 h at 37 °C. Formazan crystals were dissolved with acidified isopropyl alcohol (100 μL) and SDS (3%, 20 μL). Absorption was measured at 570 nm and background signals at 670 nm were subtracted (Spectramax M2 plate reader). Cells treated with empty vector LPXs were used as reference (100% cell viability). Terfenadine (20 μM) was used as positive control. Results are shown as means ± S.D. of $n = 5$ experiments.

4.1.14. Intracellular ATP content

Intracellular ATP content was analyzed using the CellTiter Glo Luminescent cell viability assay (Promega) in accordance with the manufacturers recommendation as described previously [60]. In brief,

100 μL of assay buffer were added to each 96-well (TPP) containing 100 μL of complete culture medium. Samples were incubated for 12 min at room temperature under light protection and luminescence was measured using an Infinite M200PRO plate reader (Tecan). Intracellular ATP content was normalized to empty vector-LPX treated control cells. 0.1% Triton-X100 was used as positive control. Results are shown as means ± S.D. of $n = 3$ replicates.

4.1.15. Kinetic cell viability assay

Changes in cell viability over time were monitored using the RealTime-Glo™ MT Cell Viability Assay (Promega). In brief, cells were seeded in 96-well plates (TPP) and transfected as described above. 100 μL of culture medium were removed 8 h post transfection and MT Cell Viability Substrate and NanoLuc® Enzyme were added at a concentration of 1× at a total volume of 200 μL per well. At indicated time points, luminescence was recorded using an Infinite M200PRO plate reader (Tecan). Values were normalized to empty vector-LPX treated control cells. Results are shown as means ± S.D. of $n = 4$ experiments.

4.1.16. Kinetic apoptosis assay

Apoptosis was detected by using the prototype RealTime-Glo™ Annexin V Apoptosis Assay (Promega). In brief, cells were seeded in 96-well plates (TPP) and transfected as described above. After 8 h of incubation with LPXs, 100 μL of culture medium was removed. Necrosis Detection Reagent, $CaCl_2$, Annexin V-SmBiT, Annexin V-LgBiT, and RT substrate were added. At indicated time points, luminescence and fluorescence (Ex: 488 nm, Em: 525 nm) were measured using an Infinite M200PRO plate reader (Tecan) and increase in apoptosis compared to empty vector-LPX treated control cells was calculated. Results are shown as means ± S.D. of $n = 3$ experiments.

4.1.17. Kinetic cytotoxicity assay

Cytotoxicity was determined using the CellTox™ Green Cytotoxicity Assay (Promega). Briefly, cells were seeded in 96-well plates (TPP) and transfected as described above. 100 μL of culture medium were removed 8 h post transfection and CellTox™ Green Dye was added. At indicated time points, fluorescence was measured using an Infinite M200PRO plate reader (Tecan; Ex: 513 nm, Em: 532 nm). Cytotoxicity is expressed as fold change as compared to empty vector-LPX treated control cells. Results are shown as means ± S.D. of $n = 3$ experiments.

4.1.18. Propium iodide (PI) staining

Cells were seeded in a 96-well plate (TPP) and were transfected with GFP or NS1-GFP as described above. After 72 h, PI (Sigma) was added at a final concentration of 500 nM for 5 min and cells were washed with D-PBS. Fluorescence was analyzed using a FV1000 confocal microscope (Olympus) using a 10× water immersion objective (NA 0.4, Olympus, Ex: 488 nm and 559 nm, Em: 520 nm and 619 nm, respectively). Fluorescence signals were quantified using ImageJ 1.46 software (National Institutes of Health). Lower particle threshold was set to 20 pixels. Percentage of dead cells was calculated by dividing counted particles in PI channel by the sum of particles counted in GFP and PI channel. Results are shown as means ± S.D. of $n = 4$ experiments.

4.1.19. Annexin V/PI staining

Apoptotic and necrotic cells were stained using the Dead Cell Apoptosis Kit (Thermo Scientific). In brief, cells were detached using 0.25% trypsin-EDTA (Thermo Scientific), washed once, and centrifuged (400 xg, 5 min, 4 °C). Cell pellets were resuspended in 100 μL Annexin V staining buffer (5 μL Alexa Fluor® 488 Annexin V and 95 μL of 1× Annexin-binding buffer) and incubated for 15 min. Then, PI was added to a final concentration of 0.7 μg mL^{-1} and cells were incubated for additional 15 min at room temperature and protected from light. Fluorescence was then analyzed by flow cytometry using a FACS Canto II flow cytometer (Becton Dickinson, Ex: 488 nm and 561 nm, Em: FL1 (505LP – 530/30 nm) and FL5 (586/15 nm), respectively). To evaluate the percentage of apoptotic and necrotic cells, Flow Jo VX software (TreeStar) was used. Results are shown as means ± S.D. of $n = 4$ experiments.

4.1.20. Detection of apoptosis in western blot

Cells were seeded in 6-well plates (TPP) and transfected as described above. Cells were washed with ice-cold D-PBS, lysed with RIPA buffer (50 nM Tris-HCL pH 7.4, 150 mM NaCl, 1% Triton X-100, 0.5% sodium deoxycholate, 0.1% sodium dodecylsulfate, and 1 mM EDTA) containing 1× protease inhibitor cocktail (Roche Diagnostics) for 15 min under constant agitation. Proteins were collected by centrifugation (15700 xg, 10 min, 4 °C) and protein concentrations were determined by Pierce BCA Protein Assay Kit (Thermo Scientific) according to the manufacturers' recommendation. Equal amounts of protein were loaded and separated on 4–12% bis-tris gradient gels (Invitrogen) using MOPS SDS running buffer (Invitrogen). After separation, proteins were transferred to nitrocellulose membranes (Bio-Rad) using the Trans-Blot Turbo Transfer System (Bio-Rad). Membranes were washed once with PBS-T for 5 min and subsequently blocked with 5% skim milk for 1 h. They then were washed with PBS-T and incubated overnight with primary antibody at 4 °C. Antibodies for detection of caspase 3, caspase 9, and PARP were from Cell Signaling Technologies. Membranes were washed three times with PBS-T and were incubated with an HRP conjugated secondary antibody at room temperature for 1 h prior to protein detection by luminescence using Western ECL Blotting Substrates (Bio-Rad) and analysis using the Fusion Pulse TS device from Vilber Lourmat. Before reprobing the membranes with another antibody, they were stripped for 15 min with Restore™ PLUS Western Blot Stripping Buffer (Thermo Scientific). Detection of GADPH (Santa Cruz Biotechnology) was used to confirm uniformity of loading and for normalization. Results are shown as means ± S.D. of $n = 3$ experiments.

4.1.21. Caspase 3 and 7 activation assay

Caspase 3 and 7 activation was analyzed using Caspase-Glo 3/7 Assay (Promega) in accordance with the manufacturer's recommendation. Briefly, at indicated time points, 67 μL of freshly prepared Caspase-Glo 3/7 Reagent was added to each 96-well (TPP) to a total volume of 135 μL. Plates were incubated for 60 min at room temperature. Luminescence was measured using an Infinite M200PRO plate reader (Tecan). Results were normalized to empty vector-LPX treated control cells and are expressed as mean fold caspase activation. Results are shown as means ± S.D. of $n = 3$ experiments.

4.1.22. DNA fragmentation analysis

Hep3B cells were seeded in 10 cm plates (TPP) and transfected. DNA was isolated at indicated time points using the Apoptotic DNA-Ladder Kit (Roche Diagnostics) as described by the manufacturer. DNA fragments were separated by agarose gel electrophoresis, stained with ethidium bromide (Roth) and analyzed using an imaging doc system (Bio-Rad Laboratories). Results are shown as means ± S.D. of $n = 3$ experiments.

4.1.23. Analysis of intracellular superoxide

Real-time analysis of reactive oxygen species (ROS) and superoxide induction was performed using the total ROS/Superoxide detection kit (Enzo Life Sciences). In brief, cells were seeded in 6-well plates (TPP) and transfected as described above. Cells were washed once with D-PBS and were detached using 0.25% trypsin/EDTA (Gibco). Cells were resuspended in 1 mL of complete culture medium, centrifuged (400 xg, 5 min, room temperature), and washed once with 1× wash buffer (provided by manufacturer). Cell suspensions were incubated with either 500 μL of oxidative stress detection reagent or superoxide detection reagent at a final concentration of 2 μM for 30 min at 37 °C. Cells were then analyzed by flow cytometry using a FACS Canto II flow cytometer (Becton Dickinson, Ex: 488 nm and 561 nm, Em: FL1 (505LP-530/30 nm) and FL6 (600LP-610/10 nm), respectively). Results were

analyzed using Flow Jo VX software (TreeStar). Results are shown as means ± S.D. of $n = 3$ experiments. Cells were subsequently analyzed using confocal microscopy. Nuclei were stained using Hoechst 33342 (Sigma). Cells were washed with D-PBS, centrifuged (400 xg, 5 min, room temperature), and mounted on cover slips using ProLong Gold (Molecular Probes). Cells were analyzed using a FV1000 confocal laser scanning microscope (Olympus) equipped with a 60× oil immersion objective (NA 1.42, Olympus). Ex: 405 nm, 488 nm, and 559 nm, Em: 425–475 nm, 500–545 nm, and 575–620 nm, respectively. Results were normalized to GFP-LPX treated control cells.

4.1.24. DNA damage analysis using gamma-H2AX

Phosphorylated histone 2AX levels were analyzed to detect DNA double strand breaks. Immunofluorescence staining was performed as described above. After blocking, cells were incubated with an anti-gamma H2AX (phospho S139) antibody (ab11174, Abcam). Hoechst 33342 and H2AX staining were analyzed using a FV1000 confocal microscope (Olympus) using a 60× oil immersion objective (NA 1.42, Olympus). Ex: 405 nm and 488 nm, Em: 425–575 nm and 500–545 nm, respectively. Alternatively, gamma-H2AX was analyzed by western blot. Cells were seeded in 6 well plates (TPP), transfected using LPXs and proteins were isolated, and transferred to PVDF membranes as described above. Membranes were incubated with an anti-gamma H2AX (phospho S139) antibody (ab11174, Abcam) over night at 4 °C in 5% skim milk in TBS-T, washed three times with TBS-T, and incubated with horseradish-peroxidase-conjugated secondary antibody for 60 min at room temperature. Proteins were detected using a ChemiDoc imaging system (Bio-Rad) after incubation with Pierce ECL Western Blotting Substrate (Thermo Scientific) Equal loading was confirmed by staining for beta actin (Santa Cruz). Cells treated with empty vector-LPXs were used as negative control.

4.1.25. Analysis of gene expression after NS1-LPX treatment by next generation sequencing

Cells were plated in 6 well plates (TPP) and transfected with empty vector-LPXs or NS1-LPXs. After 24 h or 48 h, RNA was extracted with Trizol reagent (Thermo Scientific) according to the manufacture's recommendation and RNA was purified using the miRNAeasy kit (Qiagen) and quantified with the Qubit RNA HS assay kit (Invitrogen). Library preparation was performed using the Ion AmpliSeq™ Transcriptome Human Gene Expression Research Panel (Life Technologies) following the manufacturers' instructions. The AmpliSeq™ Transcriptome Human Gene Expression Research Panel was designed to target 18,574 coding genes and 2,228 non-coding genes based on UCSC hg19 annotation allow amplification-based capture and sequencing of coding regions of 50 cancer-related genes (Thermo Scientific). First, 10 ng of DNase-treated total RNA was reverse transcribed using the SuperScript™ VILO™ cDNA Synthesis Kit (Life Technologies). cDNA was then mixed with the primer pool and the Ion AmpliSeq™ HiFi master mix (Thermo Scientific) and target enrichment was performed by an incubation at 99 °C for 2 min, followed by 12 cycles of 99 °C for 15 s and 60 °C for 16 min. The PCR products were then treated with 2 μL FuPa reagent (Ion AmpliSeq™ Library Kit Plus, Life Technologies) and incubated at 50 °C for 10 min, followed by 10 min incubation at 55 °C, and, finally, 20 min incubation at 60 °C to partially digest the primer sequences. Amplicons were ligated to IonXpress barcoded adapters for 30 min at 22 °C, followed by 5 min at 72 °C using the IonXpress™ Barcode Adapters kit (Life Technologies). Lastly, barcoded libraries were purified using Agencourt® AMPure® XP reagents (Beckman Coulter). The library concentration was determined using the Ion Library Quantitation Kit (Life Technologies) and library quality was assessed using the Bioanalyzer 2100 (Agilent Technologies). Libraries were diluted to a concentration of 75 pM and pooled before loading on the Ion Chef System for automated template prep and chip loading using the Ion S5 540 Chef Kit (Thermo Scientific). Loaded Ion 540 chips were sequenced using the Ion S5XL system (Thermo Scientific). Raw data (BAM files) for each sample were processed for the alignment of sequencing reads with the panel specific reference (hg19 AmpliSeq Transcriptome ERCC v1, tmap-f3) using the Torrent Suite software v5.2.2 (Life Technologies). The analysis pipeline also included signal processing, base calling, quality score assignment, adapter trimming, PCR duplicate removal and control of mapping quality. The ampliSeqRNA analysis plugin (Torrent Suite software, Life Technologies) was used to assess mapping statistics of each sample. This analysis showed that the number of reads that mapped to the reference transcriptome was similar between all eight samples, ranging from 16,062,159 to 19,201,295 (Table S2). Valid reads (*i.e.* reads that could be aligned to a target region and passed QC filters such as minimum alignment length) ranged between 93.8% and 95.4% of total mapped reads (Table S2). The proportion of targets that had at least 10 assigned reads ranged from 60.4% to 66.3%. Group comparison was performed with the Qlucore software using a q value of 0.01 for each comparison. For pathway analysis, Ingenuity Pathway Analysis software (Qiagen) was used. Results are shown as means ± S.D. of $n = 2$ experiments.

4.1.26. Determination of PDK1 levels in liver cancer cells

Total PDK1 expression levels in liver cancer-derived cell lines were quantified using the Human Total PDK1 ELISA Kit (RayBio). HepG2, HuH7, and Hep3B cells were seeded as described above and cell lysates were prepared according to the manufacturer's recommendation. A rabbit anti-pan-PDK1 antibody was used for detection of total PDK1 levels and signals were normalized to total protein concentrations determined by Pierce BCA Protein Assay Kit (Thermo Scientific). Results are shown as means ± S.D. of $n = 3$ replicates.

4.1.27. Influence of PDK1 on NS1 toxicity

To study the influence of PDK1 activation on NS1 toxicity, cells were transduced with constitutively active PDK1:S138E (PDK1:S138E mimics phosphorylation of PDK1-S135 resulting in constitutive active PDK1) using recombinant adeno-associated viruses (JPF Nüesch, German Cancer Research Institute, DKFZ, Heidelberg, Germany) as described previously [29]. In brief, cells were seeded in 96-well plates (TPP) as described above and transfected with rAAVs (10^4 genomes per cell). Cells were incubated 24 h post transduction with GFP or NS1-GFP-LPXs for 72 h. Dead cells were identified by a PI staining as described above. Results are shown as means ± S.D. of $n = 3$ replicates.

4.1.28. Analysis of PKC eta nuclear colocalization

Intracellular PKC eta localization was analyzed to show nuclear interaction with NS1. Immunofluorescence staining was performed as described above. After blocking, cells were incubated with an anti-PKCη antibody (rabbit polyclonal, sc-136036, Santa Cruz Biotechnology) and monoclonal primary anti-NS1 antibody (JPF Nüesch, German Cancer Research Center DKFZ, Heidelberg, Germany). Hoechst 33342, PKCη and NS1 staining were analyzed using a FV1000 confocal microscope (Olympus) using a 60× oil immersion objective (NA 1.42, Olympus). Ex: 405 nm, 488 nm, 633 nm. Results are shown as means ± S.D. of $n = 5$ replicates.

4.1.29. RNA microarray and tissue microarray of patient samples

Patients' specimens with comprehensive clinicopathological data records were obtained from the Institute of Pathology, University Hospital of Basel, Switzerland. HCC diagnosis was verified by pathological examination. Samples were from patients, which had not yet received treatments before biopsy collection. Tumor differentiation was defined according to Edmondson's grading system. Only biopsies containing at least 50% tumor cells and no necrotic area were used in this study. Roughly, 60% of patients whose specimens were used for tissue microarray construction underwent surgical resection without prior treatment for HCC, and the remaining were collected from autopsy cases. Samples were obtained with permission of the ethics committee of the University Hospital of Basel. Statistical analysis was performed as described

previously [61]. In brief, the χ2-test and Fisher's exact test for non-parametric variables were used. All tests were two-sided and $P < 0.05$ was considered to be statistically significant. Analysis was performed using GraphPad Prism software version 6 (GraphPad).

4.1.30. Detection of PDK1 mRNA levels in human liver biopsies by RNA microarray

PDK1 mRNA expression was assessed in 64 liver specimens including patient samples of different ethology such as alcohol-related HCC ($n = 30$), no virus/no alcohol-related HCC ($n = 5$), hepatitis B or C virus -related HCC ($n = 24$) and normal healthy liver specimens (n = 5) using the GeneChip®Human Gene 1.0ST arrays (Affymetrix) as previously described [62]. None of the patients received any therapeutic treatment before the biopsy. RNA for the microarray was isolated and handled as previously described [61]. Extracted RNA quality and quantity were analyzed with the Bioanalyzer 2100 using the RNA6000 Chip (Agilent Technologies). DNAse-treated total RNA (270 ng) was subjected to target synthesis using the WT Expression kit (Ambion) following standard recommendations. Then, the array was hybridised. The GeneChips were scanned with an Affymetrix GeneChip Scanner 3000 (Affymetrix). DAT images and CEL files of the microarrays were generated using Affymetrix GeneChip Command Control version 4.0 (Affymetrix). CEL files were imported into Qlucore software (Qlucore), normalized using Robust Multichip Average (RMA) prior to principal component analysis. Quantile normalization and data processing were performed using the GeneSpringGXv11.5.1 software package (Agilent Technologies). The gene signature value was assessed using the BRB-ArrayTool version 4.3.2 (National Institutes of Health).

4.1.31. Detection of PDK1 protein levels in human liver biopsies by tissue microarray

PDK1 protein levels were investigated by immunohistochemistry using a liver tissue microarray. The TMA was constructed as previously described by Baumhoer et al. using a total of 446 tissue specimens from both HCC and non-neoplastic liver tissue samples [63]. For evaluations of PDK1 protein expression, 246 specimens were suitable for analysis including 50 normal liver, 133 HCC, and 57 cirrhotic tissue specimens. Causes of exclusion were either the absence of tissue punch or poor staining quality. TMA sections (4 μm thick) were immuno-stained with an anti-PDK1 primary antibody (EP569Y (ab52893), Abcam) at a dilution of 1:100, followed by an HRP-conjugated secondary antibody using a Ventana system (Roche Diagnostics). Finally, the slides were stained with hematoxylin and eosin. PDK1 protein immunoreactivity was scored semi-quantitatively by evaluating the staining intensity as described by Allred et al. 6 (0, negative for PDK1; 3, highest intensity of PDK1) [64]. Clinico-pathological data of healthy liver specimen and the different HCC subsets are summarized in Table S5 and S6.

4.1.32. Immunohistochemical (IHC) staining of tumor tissue

IHC staining for cleaved caspase-3 and Ki67 was performed on 4 μm sections of FFPE tissue using primary antibodies anti-cleaved caspase-3 (Asp175) (Cell Signaling; #9661, dilution 1:150, buffer pH 9.0 antigen retrieval) and anti-Ki67 (Dako; clone IR626, dilution 1:200, buffer pH 6.0 antigen retrieval). Staining procedures were performed on a Leica Bond III autostainer using Bond ancillary reagents and a Refine Polymer Detection system according to the manufacturer guidelines. Immunoreactivity for Ki67 was performed semi-quantitatively as the number of positive tumor cells over the total number of tumor cells as previously described [65]. All slides were evaluated by a trained pathologist (LMT). Tumors were classified into lowly- or highly-proliferative based on Ki67 positive cells in accordance to the St. Gallen's guidelines as previously described [66]. The staining intensity of cleaved caspase-3 was classified using a numerical scale (0, no expression; 1–2, weak expression; 3, moderate expression; 4, strong expression and 5, very strong expression). All scoring was performed on at least three random fields using a 20× objective.

4.1.33. Quantification and statistical analysis

Statistical analysis was performed as indicated in the respective sections.

Acknowledgements

We thank R. Bartenschlager, M. Heikenwälder, and H. zur Hausen for fruitful discussions, critical editing, and revision of the manuscript, N. Zanella and T. Deigner from Charles River Discovery Research Services Germany GmbH for the support with xenograft experiments, A. Ríos Quiroz and F. Stump for support with NTA measurements, and HE. Meyer zu Schwabedissen and C. Ferreira for support with PCR and western blot experiments. The research project was supported by the Swiss National Science Foundation (SNSF) Grants No. 183923 (D.W.) and Sinergia CRSII5_180257 (J.H.) and the Novartis Foundation (D.W.). S.P. acknowledges the support from the SNSF (Ambizione grant, No. PZ00P3_168165) and Swiss Cancer League (Oncosuisse, KFS-3995-08-2016). The authors declare no competing financial interests.

Appendix A. Supplementary data

Supplementary data to this article can be found online at https://doi.org/10.1016/j.jconrel.2021.04.023.

References

[1] R.L. Siegel, K.D. Miller, A. Jemal, CA Cancer J. Clin. 68 (2018) 7.
[2] J. Balogh, D. Victor, E.H. Asham, S.G. Burroughs, M. Boktour, A. Saharia, X. Li, R. M. Ghobrial, H.P. Monsour, J. Hepatocell. Carcinoma 3 (2016) 41.
[3] A. Flores, J.A. Marrero, Clin. Med. Insights Oncol. 8 (2014) 71.
[4] S. Grimm, Adv. Exp. Med. Biol. 818 (2014) 1.
[5] H. Fukuhara, Y. Ino, T. Todo, Cancer Sci. 107 (2016) 1373.
[6] A. Marchini, L. Daeffler, V.I. Pozdeev, A. Angelova, J. Rommelaere, Front. Immunol. (2019) 10, https://doi.org/10.3389/fimmu.2019.01848.
[7] M. Los, S. Panigrahi, I. Rashedi, S. Mandal, J. Stetefeld, F. Essmann, K. Schulze-Osthoff, Biochim. Biophys. Acta 1793 (2009) 1335.
[8] M. Tavassoli, L. Guelen, B.A. Luxon, J. Gäken, Apoptosis Int. J. Program. Cell Death 10 (2005) 717.
[9] C. Backendorf, A.E. Visser, A.B. De, R. Zimmerman, M. Visser, P. Voskamp, Y. H. Zhang, M. Noteborn, Annu. Rev. Pharmacol. Toxicol. 48 (2008) 143.
[10] C. Hallauer, G. Siegl, G. Kronauer, Arch. Gesamte Virusforsch. 38 (1972) 366.
[11] M. Herrero, Y. Calle, J.J. Cornelis, C. Herold-Mende, J. Rommelaere, J. R. Schlehofer, K. Geletneky, Int. J. Cancer 109 (2004) 76.
[12] C. Wrzesinski, L. Tesfay, N. Salomé, J.-C. Jauniaux, J. Rommelaere, J. Cornelis, C. Dinsart, J. Virol. 77 (2003) 3851.
[13] A.L. Angelova, K. Geletneky, J.P.F. Nüesch, J. Rommelaere, Front. Bioeng. Biotechnol. 3 (2015) 55.
[14] J.P.F. Nüesch, J. Rommelaere, Adv. Exp. Med. Biol. 818 (2014) 99.
[15] P. Caillet-Fauquet, M. Perros, A. Brandenburger, P. Spegelaere, J. Rommelaere, EMBO J. 9 (1990) 2989.
[16] X. Li, S.L. Rhode, J. Virol. 64 (1990) 4654.
[17] R. Corbau, V. Duverger, J. Rommelaere, J.P. Nüesch, Virology 278 (2000) 151.
[18] S. Mousset, Y. Ouadrhiri, P. Caillet-Fauquet, J. Rommelaere, J. Virol. 68 (1994) 6446.
[19] C. Legrand, S. Mousset, N. Salomé, J. Rommelaere, J. Gen. Virol. 73 (1992) 2003.
[20] J.P.F. Nüesch, J. Rommelaere, J. Virol. 80 (2006) 4729.
[21] K. Geletneky, J. Huesing, J. Rommelaere, J.R. Schlehofer, B. Leuchs, M. Dahm, O. Krebs, M. von Knebel Doeberitz, B. Huber, J. Hajda, BMC Cancer 12 (2012) 99.
[22] K. Geletneky, J. Hajda, A.L. Angelova, B. Leuchs, D. Capper, A.J. Bartsch, J.-O. Neumann, T. Schöning, J. Hüsing, B. Beelte, I. Kiprianova, M. Roscher, R. Bhat, A. von Deimling, W. Brück, A. Just, V. Frehtman, S. Löbhard, E. Terletskaia-Ladwig, J. Fry, K. Jochims, V. Daniel, O. Krebs, M. Dahm, B. Huber, A. Unterberg, J. Rommelaere, Mol. Ther. J. Am. Soc. Gene Ther. 25 (2017) 2620.
[23] Hum. Gene Ther. 13 (2002) 3.
[24] S. Chira, C.S. Jackson, I. Oprea, F. Ozturk, M.S. Pepper, I. Diaconu, C. Braicu, L.-Z. Raduly, G.A. Calin, I. Berindan-Neagoe, Oncotarget 6 (2015) 30675.
[25] A. Wicki, D. Witzigmann, V. Balasubramanian, J. Huwyler, J. Control. Release Off. J. Control. Release Soc. 200 (2015) 138.
[26] J. Chen, Z. Guo, H. Tian, X. Chen, Mol. Ther. Methods Clin. Dev. 3 (2016) 16023.
[27] J. Buck, P. Grossen, P.R. Cullis, J. Huwyler, D. Witzigmann, ACS Nano 13 (2019) 3754.
[28] J.A. Kulkarni, D. Witzigmann, S. Chen, P.R. Cullis, R. van der Meel, Acc. Chem. Res. 52 (2019) 2435.
[29] S. Bär, J. Rommelaere, J.P.F. Nüesch, PLoS Pathog. 11 (2015), e1004703.
[30] A. Elouahabi, J.-M. Ruysschaert, Mol. Ther. 11 (2005) 336.
[31] J.P. Nüesch, P. Tattersall, Virology 196 (1993) 637.
[32] C. Cziepluch, S. Lampel, A. Grewenig, C. Grund, P. Lichter, J. Rommelaere, J. Virol. 74 (2000) 4807.

[33] A. Doyle, M. Sherman, Curr. Hepatol. Rep. 16 (2017) 46.
[34] H. Bai, G.M.S. Lester, L.C. Petishnok, D.A. Dean, Biosci. Rep. (2017) 37, https://doi.org/10.1042/BSR20160616.
[35] M. Moehler, B. Blechacz, N. Weiskopf, M. Zeidler, W. Stremmel, J. Rommelaere, P. R. Galle, J.J. Cornelis, Cancer Gene Ther. 8 (2001) 158.
[36] J.P. Nüesch, S. Lachmann, J. Rommelaere, Virology 331 (2005) 159.
[37] J.P.F. Nüesch, J. Rommelaere, Proc. Natl. Acad. Sci. U. S. A. 104 (2007) 12482.
[38] J.M. Vanacker, V. Laudet, G. Adelmant, D. Stéhelin, J. Rommelaere, J. Virol. 67 (1993) 7668.
[39] J.K. Krady, D.C. Ward, Mol. Cell. Biol. 15 (1995) 524.
[40] C. Lorson, J. Pearson, L. Burger, D.J. Pintel, Virology 240 (1998) 326.
[41] J.P.F. Nüesch, J. Lacroix, A. Marchini, J. Rommelaere, Clin. Cancer Res. Off. J. Am. Assoc. Cancer Res 18 (2012) 3516.
[42] M. Di Piazza, C. Mader, K. Geletneky, M. Herrero Y. Calle, E. Weber, J. Schlehofer, L. Deleu, J. Rommelaere, J. Virol. 81 (2007) 4186.
[43] G. Hristov, M. Krämer, J. Li, N. El-Andaloussi, R. Mora, L. Daeffler, H. Zentgraf, J. Rommelaere, A. Marchini, J. Virol. 84 (2010) 5909.
[44] R.O. Adeyemi, D.J. Pintel, J. Virol. 86 (2012) 8328.
[45] Z. Ruiz, I.S. Mihaylov, S.F. Cotmore, P. Tattersall, Virology 410 (2011) 375.
[46] J.P.F. Nüesch, S. Lachmann, R. Corbau, J. Rommelaere, J. Virol. 77 (2003) 433.
[47] S. Lachmann, S. Bär, J. Rommelaere, J.P.F. Nüesch, Cell. Microbiol. 10 (2008) 755.
[48] J.P.F. Nüesch, S. Bär, S. Lachmann, J. Rommelaere, J. Virol. 83 (2009) 5854.
[49] R. van der Meel, E. Sulheim, Y. Shi, F. Kiessling, W.J.M. Mulder, T. Lammers, Nat. Nanotechnol. 14 (2019) 1007.
[50] H.M. Mansour, Y.-S. Rhee, X. Wu, Int. J. Nanomedicine 4 (2009) 299.
[51] L. Buscail, B. Bournet, F. Vernejoul, G. Cambois, H. Lulka, N. Hanoun, M. Dufresne, A. Meulle, A. Vignolle-Vidoni, L. Ligat, N. Saint-Laurent, F. Pont, S. Dejean, M. Gayral, F. Martins, J. Torrisani, O. Barbey, F. Gross, R. Guimbaud, P. Otal, F. Lopez, G. Tiraby, P. Cordelier, Mol. Ther. 23 (2015) 779.
[52] K. Fujita, Y. Nakai, A. Kawashima, T. Ujike, A. Nagahara, T. Nakajima, T. Inoue, C. M. Lee, M. Uemura, Y. Miyagawa, Y. Kaneda, N. Nonomura, Cancer Gene Ther. 24 (2017) 277.
[53] M.A. Aznar, N. Tinari, A.J. Rullán, A.R. Sánchez-Paulete, M.E. Rodriguez-Ruiz, I. Melero, J. Immunol. 198 (2017) 31.
[54] C.G. Zamboni, J. Green, L.J. Higgins, J. Vasc. Interv. Radiol. 26 (2015) S160.
[55] R.J. Lewandowski, J.-F. Geschwind, E. Liapi, R. Salem, Radiology 259 (2011) 641.
[56] K. Hoshino, T. Kimura, A.M. De Grand, R. Yoneyama, Y. Kawase, S. Houser, H. Q. Ly, T. Kushibiki, Y. Furukawa, K. Ono, Y. Tabata, J.V. Frangioni, T. Kita, R. J. Hajjar, M. Hayase, Gene Ther. 13 (2006) 1320.
[57] S. Fuchs, A. Battler, R. Kornowski, Nat. Clin. Pract. Cardiovasc. Med. 4 (Suppl. 1) (2007). S89.
[58] O. Moralès, A. Richard, N. Martin, D. Mrizak, M. Sénéchal, C. Miroux, V. Pancré, J. Rommelaere, P. Caillet-Fauquet, Y. de Launoit, N. Delhem, PLoS One 7 (2012), e32197.
[59] A. Ríos Quiroz, J. Lamerz, T. Da Cunha, A. Boillon, M. Adler, C. Finkler, J. Huwyler, R. Schmidt, H.-C. Mahler, A.V. Koulov, Pharm. Res. 33 (2016) 450.
[60] P. Haegler, D. Grünig, B. Berger, S. Krähenbühl, J. Bouitbir, Toxicology 336 (2015) 48.
[61] L. Quagliata, M.S. Matter, S. Piscuoglio, L. Arabi, C. Ruiz, A. Procino, M. Kovac, F. Moretti, Z. Makowska, T. Boldanova, J.B. Andersen, M. Hämmerle, L. Tornillo, M.H. Heim, S. Diederichs, C. Cillo, L.M. Terracciano, Hepatol. Baltim. Md 59 (2014) 911.
[62] Z. Makowska, T. Boldanova, D. Adametz, L. Quagliata, J.E. Vogt, M.T. Dill, M. S. Matter, V. Roth, L. Terracciano, M.H. Heim, J. Pathol. Clin. Res. 2 (2016) 80.
[63] D. Baumhoer, L. Tornillo, S. Stadlmann, M. Roncalli, E.K. Diamantis, L. M. Terracciano, Am. J. Clin. Pathol. 129 (2008) 899.
[64] D.C. Allred, J.M. Harvey, M. Berardo, G.M. Clark, Mod. Pathol. Off. J. U. S. Can. Acad. Pathol. Inc 11 (1998) 155.
[65] C. Qi, J. Cao, M. Li, C. Liang, Y. He, Y. Li, J. Li, X. Zheng, L. Wang, B. Wei, Anat. Rec. 301 (2018) 1061.
[66] S. Piscuoglio, C.K.Y. Ng, M.P. Murray, E. Guerini-Rocco, L.G. Martelotto, F. C. Geyer, F.-C. Bidard, S. Berman, N. Fusco, R.A. Sakr, C.A. Eberle, L. De Mattos-Arruda, G.S. Macedo, M. Akram, T. Baslan, J.B. Hicks, T.A. King, E. Brogi, L. Norton, B. Weigelt, C.A. Hudis, J.S. Reis-Filho, Clin. Cancer Res. Off. J. Am. Assoc. Cancer Res 22 (2016) 4045.